# Long-Lived Photoinduced Charge Separation and Redox-Type Photochromism on Mesoporous Oxide Films Sensitized by Molecular Dyads

**Pierre Bonhôte,* Jacques-E. Moser, Robin Humphry-Baker, Nicolas Vlachopoulos, Shaik M. Zakeeruddin, Lorenz Walder,§ and Michael Grätzel**

*Contribution from the Laboratoire de Photonique et Interfaces, Département de Chimie, Ecole Polytechnique Fédérale de Lausanne, CH-1015 Lausanne, Switzerland*

*Received May 19, 1998*

**Abstract:** The photoinduced charge separation in three different assemblies composed of an electron donor D and a chromophore sensitizer S adsorbed on nanocrystalline $TiO_2$ films (D−S|$TiO_2$) was investigated. In all of the systems, the sensitizer was a ruthenium(II) bis-terpyridine complex anchored to the semiconductor surface by a phosphonate group. In two of the assemblies, the donor was a 4-(*N*,*N*-di-*p*-anisylamino) phenyl group linked to the 4′ position of the terpyridine, either directly (dyad D1−S) or via a benzyl ether interlocking group (dyad D2−S). In the third system, the sensitizer and the donor (3-(4-(*N*,*N*-di-*p*-anisylamino)phenoxy)-propyl-1-phosphonate) were coadsorbed on the surface ((D3+S)|$TiO_2$). Laser flash photolysis showed that the photoinduced charge separation process follows the sequence D−S*|$TiO_2$ $\overset{1}{\rightarrow}$ D−$S^+$|($e^-$)$TiO_2$ $\overset{2}{\rightarrow}$ $D^+$−S|($e^-$)$TiO_2$ $\overset{3}{\rightarrow}$ D−S|$TiO_2$ Resonance Raman spectroscopy indicates that in the excited assemblies D2−S*|$TiO_2$ and (D3+S*)|$TiO_2$, one electron is promoted from the metal center to the terpyridine ligand linked to the semiconductor, whereas in the system D1−S*|$TiO_2$ the excited electron is located on the ligand linked to the donor. The quantum yield of charge separation (steps 1 and 2) was found to be close to unity for the two former assemblies but only 60% for the latter one. In all three cases, the electron injection was very fast (<1 ns), and the hole transfer to the donor was fast (10−20 ns). The half-lifetime of the charge separated state (step 3) was 3 $\mu$s for ($D3^+$+S)|($e^-$)$TiO_2$, as in the model system $S^+$|($e^-$)$TiO_2$; it was 30 $\mu$s in $D1^+$−S|($e^-$)$TiO_2$ and 300 $\mu$s in $D2^+$−S|($e^-$)$TiO_2$. Electrodes made of any of the surface-confined dyads on conducting glass display a strong redox-type photochromism. When a positive potential (+0.5 V vs NHE) is applied to the electrode, charge recombination (step 3) is blocked. As a result, the visible absorption spectrum of the electrode changes, due to the appearance of the absorption feature of the oxidized donor ($\lambda_{max}$ = 730 nm). Return to the reduced state is achieved by electron injection through the conduction band of the $TiO_2$ under forward bias (−0.5 V). None of the assemblies D1−S|$TiO_2$ and D2−S|$TiO_2$ gave better photovoltaic performances than the model system S|$TiO_2$. This was attributed in the first case to the low injection efficiency and, in the second case, to an additional short-circuiting pathway constituted by the charge percolation inside the molecular monolayer and to the underlying conducting glass, as previously observed with monolayers of the donor D3 (Bonhôte, P.; Gogniat, E.; Tingry, S.; Barbé, C.; Vlachopoulos, N.; Lenzmann, F.; Comte, P.; Grätzel, M. *J. Phys. Chem. B* **1998**, *102*, 1498−1507).

## Introduction

Understanding light-induced charge separation in natural or artificial molecular systems and designing such systems able to efficiently convert light into chemical or electrical energy is a fascinating challenge for contemporary chemistry. Up to now, charge separation resulting from light absorption by molecular chromophores has been studied, exploiting the following two parallel strategies: on one hand, numerous molecular assemblies of donors (D), chromophores (S), and acceptors (A) in many variations have been synthesized, forming dyads, triads, tetrads, or even pentads, to achieve charge separation in solution or in monolayers.[1,2] In most cases, the studied supramolecular entities were aiming at mimicking the natural photosynthetic reaction centers and therefore incorporated porphyrins as the chromophore.[2] On the other hand, charge separation at chromophore−semiconductor interfaces (heterodyad S|A) exploited on films of nanocrystalline metal oxides has allowed the development of efficient dye-sensitized nanocrystalline solar cells.[3] Combining the intramolecular with the interfacial light-induced charge separation strategies is expected to increase the light-to-electricity conversion yield of the photovoltaic systems.

In the dye-sensitized nanocrystalline solar cells, the sensitizer

§ Present address: Institut für Chemie, Barbarastrasse 7, 49069 Osnabrück, Germany.

(1) (a) Balzani, V.; Scandola, F. *Supramolecular Photochemistry*; Ellis Horwood: New York, 1991. (b) Lehn, J.-M. *Angew. Chem.* **1990**, *102*, 1347 and references cited in ref 6.

(2) (a) Osuka, A.; Marumo, S.; Mataga, N.; Taniguchi, S.; Okada, T.; Yamazaki, I.; Nishimura, Y.; Ohno, T.; Nozaki, K. *J. Am. Chem. Soc.* 1996, *118*, 155−168 (b) Wiederrecht, G. P.; Niemczyk, M. P.; Svec, W. A.; Wasielewski, M. R. *J. Am. Chem. Soc.* **1996**, *118*, 81−88 (c) Wasielewski, M. R. *Chem. Rev.* 1992, *92*, 435. (d) Connolly, J. S.; Bolton, J. R. In *Photoinduced Electron Transfer, Part D;* Fox, M. A., Chanon M., Eds; Elsevier: Amsterdam, 1988; p 303. (e) ibid. *Part A;* p 161. (e) Harrimann, A.; Odobel, F.; Sauvage, J.-P. *J. Am. Chem. Soc.* **1994**, *116*, 5481−5482. (f) Collin, J.-P.; Harrimann, A.; Heitz, V.; Odobel, F.; Sauvage, J.-P. *J. Am. Chem. Soc.* **1994**, *116*, 5679−5690.

10.1021/ja981742j CCC: $18.00 
Published on Web 01/27/1999

is grafted by a suitable anchoring group (carboxylate,[3c] phosphonate,[3e,f] salicylate,[4] acetylacetonate[5]) on the surface of a semiconducting mesoporous oxide. Light excites the dye ($S|TiO_2 \rightarrow S^*|TiO_2$), which then injects an electron into the conduction band of the semiconductor ($S^*|TiO_2 \rightarrow S^+|(e^-_{cb})TiO_2$). The reduced state S is regenerated by a reversible redox mediator M present in the cell electrolyte. The maximal voltage delivered by the device corresponds to the difference between the quasi-Fermi level of the electrons in the semiconductor and the redox potential of the mediator. A higher cell voltage can hence be obtained either by lowering the quasi-Fermi level or by raising the redox potential of the $M/M^+$ couple. Under open circuit, for a given semiconductor, the quasi-Fermi level in the cell depends on the electron concentration in the conduction band. This concentration relaxes to a steady state where the electron injection flux equals the electron escape flux. The escape flux is composed of two contributions: the electron−sensitizer recombination flux ($S^+|(e^-_{cb})TiO_2 \rightarrow S|TiO_2$) and the electron leak to the mediator in the contacting electrolyte ($M^+ + (e^-_{cb})TiO_2 \rightarrow M + TiO_2$). Lowering the quasi-Fermi level by reducing the former flux requires a lengthening of the lifetime of the charge-separated state $S^+|(e^-_{cb})TiO_2$. If alternatively, an improved solar cell voltage is to be achieved by raising the redox potential of the mediator, the same requirement applies. In fact, the higher redox potential results in a reduced driving force for the regeneration of the dye ($S^+ + M \rightarrow S + M^+$) which will be accompanied, in the normal Marcus region, by a reduced rate. If this rate decreases, the competitive recombination flux increases, unless, again, the lifetime of the charge-separated state $S^+|(e^-_{cb})TiO_2$ is prolonged. For a longer lifetime, it is obviously necessary to remove the hole on $S^+$ away from the semiconductor surface. This can be achieved by replacing the simple chromophoric sensitizer S by a dyad sensitizer S−D in which D is an electron donor possessing a redox potential lower than that of the sensitizer but higher than that of the redox mediator. Consequently, after electron injection, the hole will be transferred from $S^+$ toward D ($D-S^+|(e^-_{cb})TiO_2 \rightarrow D^+-S|(e^-_{cb})TiO_2$). The recombination $D^+-S|(e^-_{cb})TiO_2 \rightarrow D-S|TiO_2$ is expected to be slower than the recombination $S^+|(e^-_{cb})TiO_2 \rightarrow S|TiO_2$, because of the exponential decay of the electron-transfer rate $k_{ex}(r)$ with the distance $r$, according to eq 1

$$k_{ex}(r) = k^0_{ex} \exp(-\beta(r - r_0)) \qquad (1)$$

in which $k^0_{ex}$ is the rate at the closest distance $r_0$, and $\beta$ is the damping factor of the electron transfer. The whole system $D-S|TiO_2$ constituted by the dyad adsorbed on the semiconductor, considered as an acceptor, will be referred to as *heterotriad.*

For the dyad, we first chose a structure that was already known to display light-induced charge separation in solution and that was moreover linear and rigid, affording the best chances to obtain on the $TiO_2$ surface a heterotriad fulfilling the above-described expectation. The dyad studied by Collin et al. (daap-terpy)Ru(ttp)$^{2+}$, where daap-terpy is 4′-[(*N*,*N*-di-*p*-anisylamino) phenyl)]-2,2′:6′,2″-terpyridine and ttp is 4′-*p*-tolyl-2,2′:6′,2″-terpyridine, appeared thus to be an excellent model compound.[6] The excited ruthenium−terpyridine chromophore is known to efficiently inject electrons into $TiO_2$ [3e,f] and not to undergo dissociation as do the excited ruthenium−pyridine complexes. [7] The triarylamine subunit chosen as donor moiety forms very stable cation radicals. [8] The phosphonate group in dyad **1** allows it to be firmly anchored at the $TiO_2$ surface. [3e,f] A second dyad (**2**) was synthesized in which the distance between the donor and the sensitizer is larger. Finally, the phosphonated triarylamine **3** was also prepared in order to study *bimolecular* heterotriads formed by surface coadsorption of such a donor and a ruthenium−terpyridine sensitizer (**4**, **5**). We report here on the synthesis, electrochemistry, electronic absorption, and emission spectroscopy, resonance-Raman spectroscopy of dyads **1** and **2** and of the separated redox system composed of **3** and a sensitizer, as well as on photoelectrochemistry and photodynamics of the related heterotriads formed by adsorption of these assemblies on $TiO_2$. All the heterotriads **1**$|TiO_2$, **2**$|TiO_2$, and **3**+S$|TiO_2$ display redox-type photochromism. To our knowledge, the only related phenomenon hitherto described is the UV light-induced photochromism of Prussian blue on flat $TiO_2$.[9]

Shortly before we reported preliminary results concerning dyad **1**,[10] a paper by Argazzi et al. [11] was published in which the authors described the performance of a nanocrystalline solar cell incorporating a molecular dyad based on ruthenium bipyridine as a sensitizer and phenothiazine as a donor. The aim was the same as ours, i.e., lengthening the lifetime of the charge-separated state $S^+|(e^-_{cb})TiO_2$ in order to lower the quasi-Fermi level and to gain potential, and this appears to have been achieved. No photochromism was observed, owing to the overlap of the visible absorption bands of oxidized phenothiazine and of the sensitizer.

## Experimental Section

**Synthesis.** Dry solvents for synthesis were the *absolute, over molecular sieve* quality from Fluka. Water content was measured before use by Karl-Fisher automatic titration using a Metrohm 684 KF coulometer. *tert*-Butyl methyl ether is abbreviated TBME. Silicagel was Silicagel 60 from Fluka. Melting points were recorded on a Büchi 530 apparatus, at 1 °C/min heating rate. NMR spectra were obtained on a Bruker Spectrospin 200 MHz spectrometer. Proton chemical shifts are given versus the internal standard $Me_4Si$ or, in $D_2O$, versus DSS (sodium 3-trimethylsilyl 1-propanesulfonate-1,1,2,2,3,3-$d_6$). Diazabicyclooctane (DABCO) ($\delta$ = 2.86, s) was added to some of the triarylamine solutions in $CDCl_3$ to prevent oxidation by air. $^{31}P$ chemical shifts are given versus 85% aqueous $H_3PO_4$ as an external standard. FAB-MS spectra were obtained at the Institut de Pharmacognosie et Phytochimie of the University of Lausanne, by using a Finnigan MAT

(3) (a) Desilverstro, J.; Grätzel, M.; Kavan, L.; Moser, J.; Augustynski, J. *J. Am. Chem. Soc.* **1985**, *107*, 2988 (b) O'Reagan, B.; Grätzel, M. *Nature* **1991**, *353*, 737−739. (c) Nazeeruddin, M. K.; Liska, P.; Vlachopoulos, N.; Grätzel, M. *Helv. Chim. Acta* **1990**, *73*, 1788−1803. (d) Nazeeruddin, M. K.; Kay, A.; Rodicio, J.; Humphry-Baker, R.; Müller, E.; Liska, P.; Vlachopoulos, N.; Grätzel, M. *J. Am. Chem. Soc.*, **1993**, *115*, 6382−6390. (e) Péchy, P.; Rotzinger, F. P.; Nazeeruddin, M. K.; Kohle, O.; Zakeeruddin, S. M.; Humphry-Baker, R.; Grätzel, M. *J. Chem. Soc., Chem. Commun.* **1995**, 65−66. (f) Zakeeruddin, S. M.; Nazeeruddin, M. K.; Péchy, P.; Rotzinger, F. P.; Humphry-Baker, R.; Kalyanasundaram, K.; Grätzel, M.; Sch*kl*over, V.; Haibach, T. *Inorg. Chem.* **1997,** *36*, 5937−5946.

(4) Campus, F.; Bonhôte, P.; Grätzel, M.; Heinen, S.; Walder, L. *Sol. Energy Mater.* **1999**, *56*, 281−297.

(5) Heimer, T. A.; D'Archangelis, S. T.; Farzad, F.; Stipkala, J. M.; Meyer, G. J. *Inorg. Chem.* **1996**, *35*, 5319−5324.

(6) Collin, J. P.; Guillerez, S.; Sauvage, J. P.; Barigelletti, F.; De Cola, L.; Flamigni, L.; Balzani, V. *Inorg. Chem.*, **1991**, *30*, 4230−4238.

(7) Coe, B. J., Friesen, D. A., Thompson, D. W., Meyer, T. J. *Inorg. Chem.* **1996**, *35*, 4575−4584 and refs 39−41 therein.

(8) (a) Dapperheld, S.; Steckhan, E.; Grosse Brinkhaus, K. H.; Esch, T. *Chem. Ber.* **1991**, *124*, 2557−2567. (b) Steckhan, E. *Top. Curr. Chem.* **1987**, *142*, 3−69.

(9) DeBerry, D. W.; Viehbeck, A. *J. Electrochem. Soc.* **1983**, *130*, 249−251.

(10) Bonhôte, P.; Moser, J. E.; Vlachopoulos, N.; Walder, L.; Zakeeruddin, S. M.; Humphry-Baker, R.; Péchy. P.; Grätzel, M. *J. Chem. Soc., Chem. Commun.* **1996**, 1163−1164.

(11) (a) Argazzi, R.; Bignozzi, C. A.; Heimer, T. A.; Castellano, F. N.; Meyer, G. J. *J. Am. Chem. Soc.* **1995**, *117*, 11815−11816. The full paper was published recently: (b) Argazzi, R.; Bignozzi, C. A.; Heimer, T. A.; Castellano, F. N.; Meyer, G. J. *J. Phys. Chem. B* **1997**, *101*, 2591−2597.

TSQ 700 mass spectrometer, from a nitrobenzyl alcohol matrix, with positive ionization.

**Di-*p*-anisyl-*p*-bromophenylamine (7).** The procedure was derived from that of Bacon et al. [12] Under Ar, in a 500-mL round-bottomed flask equipped with reflux condenser and magnetic stirrer, sodium (4.03 g, 0.175 mol) freshly cut into small pieces was added to dry methanol (70 mL). After complete dissolution, the solution was concentrated by distillation of 30 mL methanol. *sym*-Collidine (Fluka, *puriss.*, 220 mL) dried over molecular sieve, copper(I) iodide (Fluka, 13.3 g, 0.070 mol), and the trisbromophenylamine **6** (Aldrich, 33.74 g, 0.070 mol) were added, and the mixture was heated to reflux with vigorous stirring for 2 h. It was then filtered while still hot, and the solvents were removed under 12 mbar in a Rotavapor. The solid residue was extracted by TBME (250 mL). The extract was washed by 1 M aqueous HCl (200 mL) and twice by water (200 mL). The organic phase was dried over $MgSO_4$ and the solvent was distilled off to leave 24.57 g of a pale yellow oil that was charged onto a silica gel column (850 g). Elution was done with heptane (15 L) and then heptane/TBME 99:1. *p*-Anisyl-di-*p*-bromophenylamine eluted first, closely followed by **7**. The trianisylamine **8** was eluted last. The fractions containing mixed mono- and dibromo compounds were purified over another 400 g of silica gel. Finally, the products were isolated by crystallization from heptane. Yield: 6.77 g (25%) **7** as a yellowish powder and 5.74 g (24%) **8** as white needles (mp 95 °C). $^1$H NMR of **7** ($\delta$ in $CDCl_3$) 7.23 (dt, 2H, $J$ = 9 and 2.2 Hz), 7.02 (dt, 4H, $J$ = 9 and 2.2 Hz), 6.81 (dt, 4H, $J$ = 9 and 2.2 Hz), 6.78 (dt, 2H, $J$ = 9 and 2.2 Hz); mp 98−99 °C.

**4-(*N*,*N*-Di-*p*-anisylamino)benzaldehyde (9).** The procedure was derived from that of Olah et al. [13] Under Ar, **7** (3.84 g, 10 mmol) was dissolved in dry THF (50 mL). The solution was cooled to −70 °C and, with stirring, *tert*-butyllithium (Aldrich, 1.5 M in pentane, 7.3 mL, 11 mmol) was slowly added by syringe, keeping the temperature below −65 °C. After 45 min, a solution of *N*-formylmorpholine (Fluka, 1.73 g, 15 mmol) in dry THF (10 mL), dried over molecular sieve, was added in one portion. The mixture was allowed to warm to room temperature After 12 h, the reaction was quenched by 1 M aqueous HCl (15 mL), and extraction was carried out by TBME (100 mL), the organic phase being washed sequentially by saturated aqueous $NaHCO_3$ and water (2 × 50 mL each). The ethereal extract was dried over $Na_2SO_4$. After solvent removal, the remaining 3.8 g of yellow oil was purified by chromatography over silica gel (150 g), eluting by heptane/TBME, 99:1 to 95:5. The fractions containing the aldehyde were yellow with blue fluorescence in UV light. Yield: 3.00 g (84%) of a yellow oil. $^1$H NMR ($\delta$ in $CDCl_3$) 9.75 (s, 1H), 7.62 (dt, 2H, $J$ = 9 and 2.2 Hz), 7.12 (dt, 4H, $J$ = 9 and 2.2 Hz), 6.88 (dt, 4H, $J$ = 9 and 2.2 Hz), 6.84 (dt, 2H, $J$ = 9 and 2.2 Hz), 3.81 (s, 6H).

**4′-[4-(*N*,*N*-Di-*p*-anisylamino)phenyl]-2,2′:6′,2″-terpyridine (L, 10).** This was prepared according to the literature procedure, [6,14] with **9** (3.18 g, 9.55 mmol), 2-acetylpyridine (Fluka, 2.31 g, 19.3 mmol), ammonium acetate (11.5 g) in acetamide (18 g). The black glassy product obtained at the end of the reaction was not treated with HBr in acetic acid, as in the tolylterpyridine synthesis, since this procedure does not lead to precipitation of the hydrobromide. Chromatography on silica gel (120 g), eluting with TBME/heptane/triethylamine, 85:14.5:0.5, afforded **10** as the second fraction, characterized by $R_f$ = 0.52 in TLC on silica gel (TBME/heptane/triethylamine, 80:19:1). Fractions containing **10** mixed with other products were rechromatographed. Final yield 0.798 g (16%). $^1$H NMR ($\delta$ in $CDCl_3$) identical to previously reported spectrum;[6] mp 201−203 °C.

**$LRuCl_3$.** This was prepared according to the usual procedure.[6,15] After filtration of the product (yield: 80%), addition of aqueous $KPF_6$ to the filtrate caused the precipitation of $RuL_2(PF_6)_2$ (**18**) (yield: 16%).

**Sodium 2,2′:6′,2″-terpyridine-4′-phosphonate (terpy$PO_3Na_2$, 11).** 4′-Diethyl phosphono-2,2′:6′,2″-terpyridine[3f] (73.8 mg, 0.20 mmol) was refluxed for 15 h in 3 M aqueous HBr (20 mL). The solvent was evaporated to dryness. The residue was dissolved in $H_2O$ (20 mL), filtered, brought to pH = 9.7 by addition of $Na_2CO_3$, and evaporated to dryness in a Rotavapor. The resulting solid was extracted with ethanol and methanol, the solvents were evaporated, leaving 134 mg of white solid containing about 47% NaBr. $^1$H NMR ($\delta$ in $D_2O$) 8.70 (d, 2H, $J$ = 5 Hz), 8.38, 8.33, and 8.29 (2 overlapping d, 4H, $J$ = 11 and 8 Hz), 8.07 (td, 2H, $J$ = 8 and 1.5 Hz), 7.57 (dd, 2H, $J$ = 5 and 7 Hz).

**L$RuterpyPO_3$ (1).** $LRuCl_3$ (74.3 mg, 0.10 mmol), **11** (67 mg, 0.10 mmol, containing 47% NaBr), triethylamine (3 mL), and ethanol (2 mL) were mixed in *N*-methylpyrrolidone (20 mL). The solution was stirred at 110 °C for 24 h. The solvent was distilled off in a Rotavapor, and the residue was dissolved in acetonitrile/water, 10:1, and purified by chromatography over silica gel, eluting with acetonitrile/water, 2:1. The bright-red fractions having $R_f$ = 0.1 in TLC on silica gel ($CH_3CN$/aqueous 0.1 M $KNO_3$, 2:1) and the absorption spectrum given in Table 2 were collected. The solvent was distilled off, and the orange solid which contained some silica from the column was dissolved in 5 mL ethanol, whereby it was separated from the $SiO_2$. Evaporation of the solvent afforded 30.0 mg **1** (32%): $^1$H NMR ($\delta$ in $CD_3OD$) 9.14 (s, 2H), overlapping with 9.14 (d, 2H, $J$ = 10 Hz), 8.80 (d, 2H, $J$ = 8 Hz), 8.63 (d, 2H, $J$ = 8 Hz), 8.10 (d, 2H, $J$ = 9 Hz), 8.00−7.90 (m, 4H), 7.47 (t, 4H, $J$ = 7 Hz), 7.27−7.17 (m, 8H), 7.11 (d, 2H, $J$ = 9 Hz), 6.97 (d, 2H, $J$ = 9 Hz), 3.84 (s, 6H); FAB-MS (nitrobenzyl alcohol matrix) $m/z$ 950.6 (calcd 949.2); UV−vis, see Table 2.

**Tris(*p*-anisyl)amine (8).** A procedure similar to the one for **7** was followed, with sodium (5.52 g, 0.24 mol), methanol (40 mL), CuI (7.60 g, 0.040 mol), the tris-bromophenylamine **6** (19.82 g, 0.040 mmol), and *sym*-collidine (250 mL). Reflux was maintained for 14 h. A first pure fraction of the product was obtained by two crystallizations from heptane (7.92 g). Distillation of the solvent from the supernatant solution afforded an oil that was shown by $^1$H NMR to contain equimolar amounts of **8** and **7**. Chromatography over silica gel (130 g) gave another 1.43 g **8** as well as 1.20 g (8%) **7**: total yield of **8**, 9.35 g (70%); $^1$H NMR ($\delta$ in $CDCl_3$) 6.96 (dt, 6H, $J$ = 9 and 2.2 Hz), 6.77 (dt, 6H, $J$ = 9 and 2.2 Hz), 3.77 (s, 9H); mp 95 °C.

**4-(*N*,*N*-di-*p*-anisylamino)phenol (12). 8** (6.70 g, 20 mmol) was dissolved in a mixture of acetic acid (42 mL), 48% aqueous HBr (30 mL), and water (5 mL). The mixture was refluxed, and the reaction was monitored by TLC on silica gel, with TBME/heptane, 1:1, as eluent. $R_f$ are the following: 0.66 (**8**); 0.50 (**12**); 0.32 (bis-*p*-hydroxyphenyl-*p*-anisylamine); 0.20 (nitrilotriphenol). After 20 min, the mixture was cooled to room temperature and concentrated in a Rotavapor under 12 mbar to 10 mL; TBME (20 mL) was added and washed twice by water (20 mL). The organic phase was dried over $MgSO_4$, and the solvent was distilled off. The remaining oil was chromatographed over silica gel (270 g), using first heptane and then heptane/TBME, 9:1 to 7:3 as eluents. **8** was eluted first, followed after several liters of eluent by **12**. Distillation of the solvent in a Rotavapor, finally under 0.1 mbar at 50 °C for 1 h, affords 2.75 g of a waxy solid that was shown by NMR to still contain 33% molar fraction of TBME. Effective yield: 38%. A 0.10 M solution in dry THF was immediately prepared for use in the next syntheses. $^1$H NMR ($\delta$ in $CDCl_3$ + DABCO) 6.98−6.65 (m, 12H), 3.77 (s, 6H), 3.22 (s, TBME), 1.19 (s, TBME).

**4′-*p*-tolyl-2,2′:6′,2″-terpyridine (13) and 4′-(*p*-bromomethylphenyl)-2,2′:6′,2″-terpyridine (14).** The compounds were prepared following the previously described procedure.[6]

**4′-(4-(*N*,*N*-di-*p*-anisylamino)phenoxymethylphenyl)-2,2′:6′,2″-terpyridine (L′ 15). 12 (**0.10 M) in dry THF (5.0 mL, 0.50 mmol) and potassium *tert*-butoxide (1.0 M) in dry THF (0.5 mL, 0.50 mmol) were mixed under Ar. After 15 min, a solution of **14** (0.201 g, 0.50 mmol) in 8 mL of dry THF was added under stirring. The solution was refluxed for 24 h; meanwhile a precipitate of KBr was formed. The solvent was removed in a Rotavapor and the solid extracted by TBME (50 mL) and water (20 mL). The organic phase was washed with water and dried over $Na_2SO_4$. The waxy solid remaining after solvent distillation was chromatographed over silica gel (11 g), eluting first by heptane/triethylamine, 99:1, and then by heptane/TBME, 100:0 to 50:50. Yield: 154 mg (48%). $^1$H NMR ($\delta$ in $CDCl_3$) 8.75 (s, 2H) overlapping in part with 8.72 (dd, 2H, $J$ = 5 and 1 Hz), 8.68 (dt, 2H, $J$ = 9 and 1 Hz), 7.93 (d, 2H, $J$ = 8 Hz), 7.89 (td, 2H, $J$ = 8 and 2 Hz), 7.57 (d, 2H, $J$ = 8 Hz), 7.36 (ddd, 2H, $J$ = 8, 5 and 1 Hz), 6.99

(12) Bacon, R. G. R.; Rennison, S. C. *J. Chem. Soc. C*, **1969**, 312−315.
(13) Olah, G. A.; Ohannesian, L.; Arvanaghi, M. *J. Org. Chem.* **1984**, *49*, 3856−3857.
(14) Spahni, W.; Calzaferri, G. *Helv. Chim. Acta* **1984**, *67*, 450−454.
(15) Sullivan, B. P.; Calvert, J. M.; Meyer, T. J. *Inorg. Chem.* **1980**, *19*, 1404−1407.

(dt, 6H, $J = 9$ and 2.2 Hz), 6.87 (dt, 2H, $J = 9$ and 2.2 Hz), 6.79 (dt, 2H, $J = 9$ and 2.2 Hz), 5.11 (s, 2H), 3.78 (s, 6H); mp 161−163 °C.

**L′RuCl$_3$.** The compound was prepared according to the usual procedure.[6,15] Yield: 86%.

**L′Ru(terpyPO$_3$) (2).** The compound was prepared by a procedure similar to the one for **1**. Elution was done with acetonitrile/water, 3:1. To remove the silica gel dissolved from the column, the product obtained after elimination of the solvent was redissolved in acetonitrile/ethanol, 1:1, and the insoluble $SiO_2$ was filtered off. **2** was isolated by precipitation from the filtrate by addition of TBME. Yield: 25%. $^1$H NMR ($\delta$ in $CD_3OD$) 9.17 (s, 2H), 9.10 (d, 2H, $J = 11$ Hz), 8.78 (d, 2H, $J = 8$ Hz), 8.65 (d, 2H, $J = 8$ Hz), 8.28 (d, 2H, $J = 8$ Hz), 7.97 (t, 4H, $J = 8$ Hz), 7.83 (d, 2H, $J = 8$ Hz), 7.47 (d, 2H, $J = 6$ Hz), 7.43 (d, 2H, $J = 6$ Hz), 7.23 (t, 4H, $J = 7$ Hz), 6.97 (s, 4H), 6.95 (d, 4H, $J = 9$ Hz), 6.84 (d, 4H, $J = 9$ Hz), 5.27 (s, 2H), 3.77 (s, 6H); FAB-MS (nitrobenzyl alcohol matrix) *m*/*z* 1056.7 (calcd 1055.2); UV−vis: see Table 2.

**(Et$_2$O$_3$Pterpy)RuCl$_3$.** The compound was prepared according to the usual procedure[15] from $RuCl_3 \cdot 3H_2O$ and 4′-diethylphosphono-2,2′:6′,2″-terpyridine ($Et_2O_3$Pterpy). Yield: 82%.

**(Me$_2$bipy)Ru(NCS)(terpyPO$_3$H) (4).** The synthesis of this complex was reported elsewhere.[3f]

**Me$_3$terpyRuterpyPO$_3$H(ClO$_4$) (5).** $Et_2O_3$terpyRuCl$_3$ (0.10 g, 0.18 mmol) and 4,4′,4″-trimethyl-2,2′:6′,2″-terpyridine ($Me_3$terpy, 60 mg, 0.22 mmol) were reacted for 4 h in refluxing DMF (30 mL). The solution was cooled to room temperature, filtered, and concentrated in a Rotavapor. Diethyl ether was added until precipitation of the complex. $^1$H NMR showed partial de-ethylation of the phosphonate. The hydrolysis was completed by refluxing for 10 h in 4 M aqueous HCl. The solvent was removed in a Rotavapor. The dry solid was redissolved in water, and the pH was raised to 6 by addition of 0.01 M aqueous NaOH and then lowered to 2.5 by addition of $HClO_4$, whereby **5** precipitated. Yield: 60 mg (40%). $^1$H NMR ($\delta$ in DMSO-$d_6$) 9.17 (d, 2H), 8.94 (s, 2H), 8.83 (d, 2H), 8.65 (d, 2H), 7.97 (d, 2H), 7.40 (d, 2H), 7.27 (t, 2H), 7.16 (d, 2H), 7.10 (d, 2H), 2.90 (s, 3H), 2.40 (s, 6H); $^{31}$P NMR ($\delta$ in DMSO-$d_6$) 3.10; UV−vis: see Table 2. An X-ray crystal structure of the compound was obtained and will be published elsewhere.

**Ru(terpyPO$_3$H$_2$)$_2$Cl$_2$ (16).** 4′-Diethylphosphono-2,2′:6′,2″-terpyridine (0.12 g, 0.32 mmol) and $RuCl_3 \cdot 3H_2O$ (0.040 g, 0.15 mmol) were reacted for 6 h in refluxing DMF (25 mL). The solution was filtered at room temperature and concentrated in a Rotavapor, and diethyl ether was added until precipitation of the complex. Hydrolysis was carried out as for **5**. The precipitate formed after cooling at room temperature of the HCl solution was isolated by filtration. Yield: 60 mg (49%). $^1$H NMR ($\delta$ in 0.02 M NaOD/$D_2O$) 8.93 (d, 2H), 8.53 (d, 2H), 7.87 (t, 2H), 7.40 (d, 2H), 7.09 (t, 2H); $^{31}$P NMR ($\delta$ in 0.02 M NaOD/$D_2O$) 7.23; UV−vis: see Table 2. Anal. Calcd. for **16**$\cdot 5H_2O$ found (calcd): C 40.6 (42.4), H 9.5 (9.5), N 3.8 (3.9).

**Diethyl 3-bromopropylphosphonate (17).** In a 50-mL two-necked round-bottomed flask equipped with a reflux condenser on one neck and a distillation head on the other, a mixture of 1,3-dibromopropane (Fluka, 20.2 g, 0.10 mol) and triethyl phosphite (Fluka, 4.15 g, 0.025 mol) was heated to 130 °C with stirring. Bromoethane distilled during 30 min. Heating was continued for another 90 min. The excess dibromopropane was removed under 12 mbar in a Rotavapor. $^1$H NMR shows no impurity in the crude product. It was however distilled over a 5-cm Vigreux column, under 0.1 mbar. **17** was collected at 57.5 °C. Yield, 3.80 g (59%). $^1$H NMR ($\delta$ in $CDCl_3$) 4.10 (t, 4H, $J = 7$ Hz), 3.48 (t, 2H, $J = 6$ Hz), 2.23−2.06 (m, 2H), 1.98−1.81 (m, 2H), 1.34 (t, 6H, $J = 7$ Hz); density at 20 °C: 1.348 g/cm$^3$.

**Sodium 3-(4-(*N*,*N*-di-*p*-anisylamino)phenoxy)-propyl-1-phosphonate (3).** Under Ar, **12** (0.10 M) in dry THF (15.0 mL, 1.50 mmol) and potassium *tert*-butoxide (0.95 M) in dry THF (1.64 mL, 1.50 mmol) were mixed. After 15 min, a solution of **17** (0.390 g, 1.50 mmol) was added under stirring, and the solution was refluxed. After 5 min, a precipitate of KBr appeared. Monitoring by TLC on silica gel (eluent: TBME) showed that after 4 h, the reaction did not progress any more (**12**: $R_f = 0.59$; **3**: $R_f = 0.22$) The mixture was diluted with TBME (30 mL) and washed twice with water (30 mL). The organic phase was dried over $Na_2SO_4$. Removal of the solvent in a Rotavapor afforded 0.90 g of crude product that was purified by chromatography over silica gel (30 g). Eluting with TBME/heptane, 33:67 to 100:0, and finally by ethyl acetate gave 0.578 g of an oil that was shown by $^1$H NMR to contain 10−20% **17**. This starting material was evaporated under 0.05 mbar at 100 °C for 1 h, leaving 0.546 g of pure ethyl ester of **3** (73%). This product (1.01 mmol) was diluted under Ar with dry $CH_2Cl_2$ (25 mL), trimethylsilyl bromide (Fluka, 1.84 g, 12 mmol) was added, and the mixture was stirred for 15 h at room temperature. The solvent and excess TMSBr were evaporated off under Ar in a Rotavapor. Fresh $CH_2Cl_2$ (20 mL) was added, and the solution was washed with water (2 × 20 mL). The organic phase was mixed with an equal volume of water, and the biphasic system was slowly neutralized by 0.1 M aqueous NaOH with gentle stirring to prevent emulsification. Water was removed from the aqueous phase in a Rotavapor, and the remaining solid was extracted with THF (20 mL). Precipitation of **3** was accomplished by addition of TBME. Yield: 0.376 g white solid (71% from the ethyl ester). $^1$H NMR ($\delta$ in $D_2O$) diethylester of **3**: 6.98−6.92 (m, 6H), 6.81−6.73 (m, 6H), 4.11 (quint. d, 4H $J = 7$ and 1.7 Hz), 3.97 (t, 2H, $J = 7$ Hz), 3.78 (s, 6H), 2.15−1.85 (m, 4H), 1.32 (t, 6H, $J = 7$ Hz); **3**: 6.92−6.75 (m, 12H), 3.96 (t, 2H, $J = 7$ Hz), 3.75 (s, 6H), 2.15−2.00 (m, 2H), 1.68−1.51 (m, 2H). Anal. Calcd. for **3**$\cdot H_2O + 3.4\%$ $NaHCO_3$ found (calcd): C 53.21 (53.38), H 5.06 (5.15), N 2.67 (2.30), O 23.45 (23.62), Na 9.70 (9.71).

**Sodium 3-(4-phenyl-phenoxy)propyl-1-phosphonate (19).** A procedure similar to the one for **3** was used**.** From 4-hydroxybiphenyl (Fluka, 0.510 g, 3.0 mmol), potassium *tert*-pentylate (1.7 M) in toluene (Fluka, 1.76 mL, 3.0 mmol) and **17** (0.777 g, 3.0 mmol), we obtained after chromatography 0.686 g of diethylester of **19** ($R_f = 0.19$ on silica gel, with TBME). For hydrolysis, this ester was dissolved in dichloromethane (20 mL) and trimethylsilyl bromide (1.90 M in $CH_2Cl_2$, 12.6 mL, 24.0 mmol) was added. After 15 h stirring at room temperature, the solvent and excess TMSBr were distilled off. Dichloromethane and water (20 mL each) were added, and the mixture was stirred. After 2 min, a white solid formed. Some more product was precipitated by addition of heptane (10 mL). The product was filtered, washed with water, and dried (yield: 493 mg). To a suspension of this solid in water (20 mL), 1.00 M aqueous NaOH (3.37 mL) was added to dissolve the solid. The solution was filtered, and the water was distilled off from the filtrate, leaving a white solid that was dissolved in methanol/water (9:1) and precipitated by slow addition of ethanol under stirring. Yield: 428 mg (42%). $^1$H NMR ($\delta$ in $D_2O$) 7.47−7.42 (m, 4H), 7.33−7.17 (m, 3H), 6.91 (dt, 2H, $J = 9$ and 2 Hz), 3.92 (t, 2H, $J = 7$ Hz), 1.84−1.68 (m, 2H), 1.40−1.23 (m, 2H). Anal. Calcd. for **19**$\cdot 1.2H_2O$ found (calcd): C 50.8 (50.4), H 5.1 (4.9), O 23.26 (23.25).

**Preparation and Characterization of the Nanocrystalline Layers.** The procedure was carried out as previously described.[16,17] The thickness of the layer was 4.5 to 5 $\mu$m, affording a roughness factor $\rho = 450-500$.[17] To remove water and organic material adsorbed during storage, the electrodes were heated to 350 °C for 30 min in an air stream. Derivatization was done by immersing the still hot (60−80 °C) electrode in a sub-millimolar solution of the relevant compound in absolute ethanol. After 12 h at room temperature, the electrodes were rinsed with absolute ethanol, dried briefly (1 min) at 100 °C, and used directly or stored in cyclohexane. At monolayer coverage, the very large surface area offered by the porous solid allowed adsorption of a considerable amount of the dyes, thus leading to high optical densities ($A_{430\ nm} \geq 0.5$). It was shown previously that a given ratio of the two phosphonates **3** and **4** (or **5**) in solution adsorbed in the same ratio on the $TiO_2$ surface.[17]

**Instrumentation.** Cyclic voltammetry, electrolyses, and photoelectrochromic experiments were carried out with a PC-controlled Ecochemie model Autolab P20 potentiostat. In all of the experiments, the reference electrode was $Ag/Ag^+$−saturated NaCl (+0.197 V vs NHE), and the counter electrode was glassy carbon. Both were separated by

(16) (a) O'Regan, B.; Moser, J.; Anderson, M.; Grätzel, M. *J. Phys. Chem.* **1990**, *94*, 8720. (b) Barbé, C.; Arendse F.; Comte, P.; Jirousek, M.; Lenzmann, F.; Shklover, V.; Grätzel, M. *J. Am. Ceram. Soc.* **1997**, *80*, 3157−3171.

(17) Bonhôte, P.; Gogniat, E.; Tingry, S.; Barbé, C.; Vlachopoulos, N.; Lenzmann, F.; Comte, P.; Grätzel, M. *J. Phys. Chem. B* **1998**, *102*, 1498−1507.

a salt bridge from the solution in contact with the working electrode. For photoelectrochromic measurements, the working electrodes were 4.8 $\mu$m $TiO_2$ on 1 $cm^2$ $SnO_2$, derivatizated in 0.5 mM solutions in EtOH for 12−15 h. The spectrophotometric measurements were effected with a HP8453 diode array spectrophotometer from Hewlett-Packard, in a 1 × 1 cm spectroelectrochemical cell. Electrolyses were carried out on carbon felt. Illumination for the photochromic measurements was done with a halogen source, through two optical fibers, using a Highlight 3001 device from Olympus, equipped with a UV filter (cutoff 420 nm). Light intensity on the electrodes was 1 ± 0.2 sun (AM 1.5).

The resonance Raman (RR) spectra were obtained using a coherent INNOVA 200K $Kr^+$ laser source and a Spex 1877 Triplemate with $N_2$-cooled CCD-1024 detection. All of the samples were prepared as 1 mM aqueous solutions stored in 1-mm i.d. glass capillaries. The sample were irradiated in a 90° geometry.

Emission spectra were recorded in a Spex Fluorolog 112 using a 90° optical geometry. The emitted light was detected with a Hamamatsu R2658 photomultiplier operated in single photon counting mode. The emission spectra were photometrically corrected using a calibrated 200-W tungsten lamp as reference source. The samples were purged with $N_2$ and the absorption spectra measured prior to each emission measurement. A dilute solution of quinine sulfate was used as a quantum yield standard.[18]

The kinetics of electron-transfer processes were examined by laser flash photolysis using dye-sensitized porous transparent $TiO_2$ films deposited on glass substrates. The surface of the sample was usually covered by a film of solvent, and protected by a thin microscope coverglass. Pulsed laser excitation was applied using a GWU BBO-C355 broad-band optical parametric oscillator pumped by a Continuum Powerlite 7030 frequency-tripled Q-switched Nd:YAG laser ($\lambda$ = 355 nm, repetition rate 30 Hz). The output of the OPO (pulse width at half-height ca. 5 ns) was typically tuned at $\lambda$ = 430 or 480 nm and attenuated to 1.5 mJ/pulse. The beam was expanded by a plano−concave lens to irradiate a large cross-section (approximately 1 $cm^2$) of the sample, whose surface was kept at a 45° angle to the excitation and to the analyzing light. The probe beam, produced by a CW 450-W Xe-arc lamp, was passed through various optics and filters, the sample, and a monochromator prior to being detected by a Hamamatsu R928 photomultiplier tube, only three dynodes of which were used. A Tektronix DSA 602A 1-GHz digital signal analyzer was employed to record the time course of the optical absorbance changes induced by pulsed laser excitation of the films. Satisfactory S/N ratios exceeding 20 were typically obtained by averaging over 10−200 laser shots. Kinetic data were finally analyzed on an Apple Power Macintosh personal computer using WaveMetrics Igor Pro software.

The photovoltaic performance of solar cells incorporating either **1**, **2**, or **5** as photosensitizers was characterized using two complementary techniques. The first method measures the current−voltage characteristic of a sandwich-type cell with platinized $SnO_2$ counter electrode under different light intensities up to AM 1.5 (or 1 Sun). The simulated solar source was a 450-W Xe lamp whose spectral output matched the AM 1.5 solar spectrum in the region of 350 to 750 nm (mismatch < 2%). Different light intensities were adjusted with neutral wire mesh attenuators. The applied potential and measured cell current was performed using a Keithley model 2400 digital source meter.[16b] The fully automated experiment was run using WaveMetrics Igor Pro. The spectral response of the cell was determined by measuring the incident photon-to-current conversion efficiency (IPCE) as a function of the wavelength[16b]

$$\mathrm{IPCE}(\lambda) = 1240(I_{sc}/\lambda\Phi) \qquad (2)$$

where $\lambda$ is the wavelength (nm), $I_{sc}$ is the current at short circuit ($mA/cm^2$) and $\Phi$ is the incident radiative flux ($W/m^2$).

## Results and Discussion

**Synthesis.** Synthesis of dyad **1** was carried out as depicted in Scheme 1. It followed in part the procedure established by Collin et al.[6] except that we found it easier to prepare the intermediate dianisylaminobenzaldehyde **9** from the commercially available tris-bromophenylamine **6** rather than from *N*,*N*′-di-*p*-anisylphenylamine. The copper (I)-catalyzed substitution of the halogen atoms by methoxy groups[12] in **6** can be well controlled by the amount of added alkoxide and reaction time. Chromatography allows the separation of the mono-, di-, and trialkoxilated products. The lithiated derivative of **7** was efficiently formylated by *N*-formylmorpholine[13] to give **9**. The building of the terpyridine moiety on the formyl group was done as previously described[6] to afford the ligand L (**10**) which reacted smoothly with $RuCl_3$ to form the complex $LRuCl_3$,[15] together with a small amount of the bis-complex LRu(II)L (**18**). The last step of the synthesis involves the displacement of three chloride ions of $LRuCl_3$ by the ligand **10**, using triethylamine as a reducing agent.

**Scheme 1**[a]

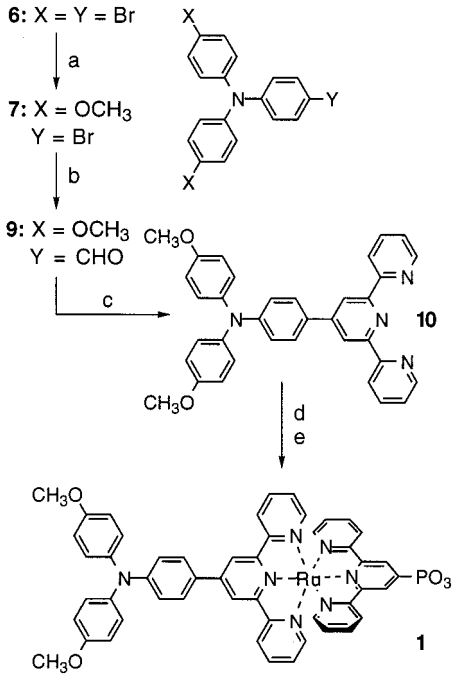


[a] 2.5 equiv of MeONa, CuI/collidine-MeOH 2 h reflux (25%); (b) *tert*-BuLi/THF, −70 °C 45 min; *N*-formylmorpholine/THF, 12 h at rt (84%); (c) 2-acetylpyridine, $NH_4CH_3COO$, $CH_3CONH_2$ (16%); (d) $RuCl_3 \cdot 3H_2O$/EtOH (80%). (e) $terpyPO_3Na_2$/NMP-$NEt_3$-EtOH 24 h 110 °C (47%).

Dyad **2** was prepared according to Scheme 2. Partial acidic hydrolysis of the trianisylamine **8** followed by chromatographic separation afforded the monophenol **12**, a key intermediate for all the syntheses of functionalized tris-alcoxyphenylamines. Bromotolylterpyridine **14** was prepared according to the previously described procedure[6] and reacted with the phenolate of **12**, to give the ligand L′ (**15**). Formation of the final ruthenium complex **2** was achieved as for dyad **1**.

The phosphonated triarylamine **3** was obtained by nucleophilic substitution between the phenolate of **12** and diethyl 3-bromopropylphosphonate **17**, followed by de-ethylation with trimethylsilyl bromide.[19] **17** was itself made by Arbusow reaction of 1,3-dibromopropane with triethyl phosphite.[20]

The $^1$H NMR chemical shifts recorded for **L**, **L**′, $terpyPO_3^{2-}$, and for the complexes **1** and **2** were attributed considering the previously reported assignments (Figure 1),[2f,21] as well as the

(18) Parker, C. A.; Rees, W. T. *Analyst (London)* **1960**, *85*, 587.

(19) Katz, H. E.; Bent, S. F.; Wilson, W. L.; Schilling, M. L.; Ungashe, S. B. *J. Am. Chem. Soc.* **1991**, *116*, 6631−6635.

(20) Arbusow, B. A. *Pure Appl. Chem.* **1964**, *9*, 307−335. Katz, H. E.; Wilson, W. L.; Scheller, G. *J. Am. Chem. Soc.* **1994**, *116*, 6636−6640.

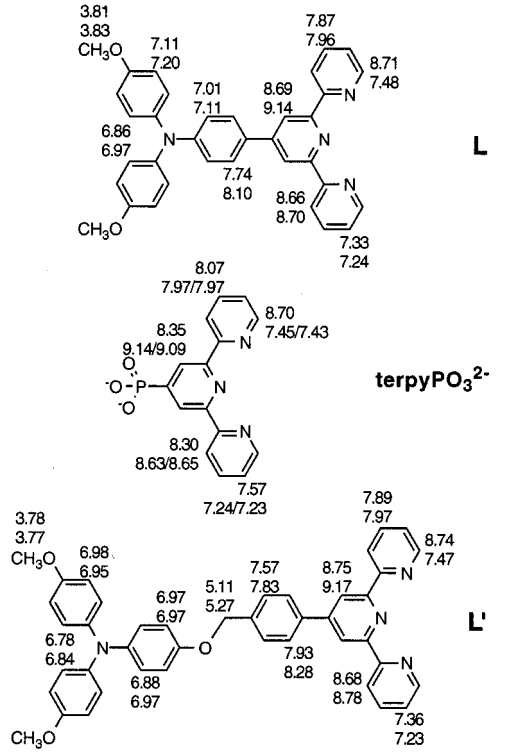


**Figure 1.** $^1$H NMR chemical shifts ($\delta$ in ppm versus $Me_4Si$) assignments for **L**, terpy$PO_3^{2-}$, and **L′**, in the isolated molecules (top value) and in the complexes **1** and **2** (bottom value; for terpy$PO_3^{2-}$: left, $\delta$ in **1** and right, $\delta$ in **2**).

observed multiplicities and coupling constants of the signals. In the free ligands **L**, the strong electronic coupling between

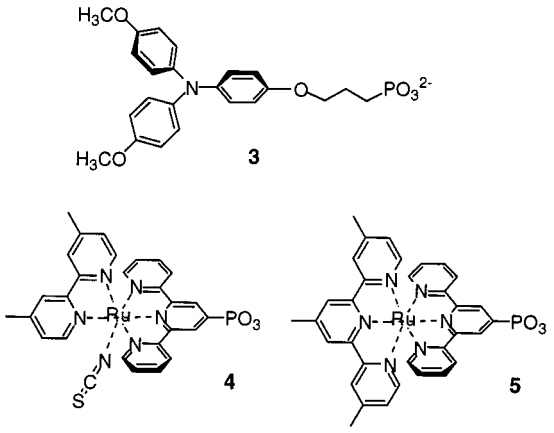


the electron donor (triarylamine) and the electron acceptor (terpyridine) shows itself by a downfield shift of the protons in the former moiety and by an upfield shift in the latter, compared to **L′**, where this coupling is much weaker. In **1**, the inductive effect of the central ion extends into the triarylamine, which is not the case in **2**, due again to the difference in the donor−chromophore couplings.

**Electrochemistry.** The electrochemical properties of the investigated systems are listed in Table 1. In accordance with previous work[6,22] the redox potentials observed close to −1 V were attributed to one-electron reduction of the terpyridine ligands and that near 1.5 V to metal-centered oxidation. For

(21) Tiecco, M.; Testaferri, L.; Tingoli, D.; Chianelli, D.; Montanucci, S. *Synthesis* **1984**, 736−738.

(22) Juris, A.; Balzani, V.; Barigelletti, F.; Campagna, S.; Belser, P.; Von Zelewsky, A. *Coord. Chem. Rev.* **1988**, *84*, 85−277.

**Scheme 2**[a]

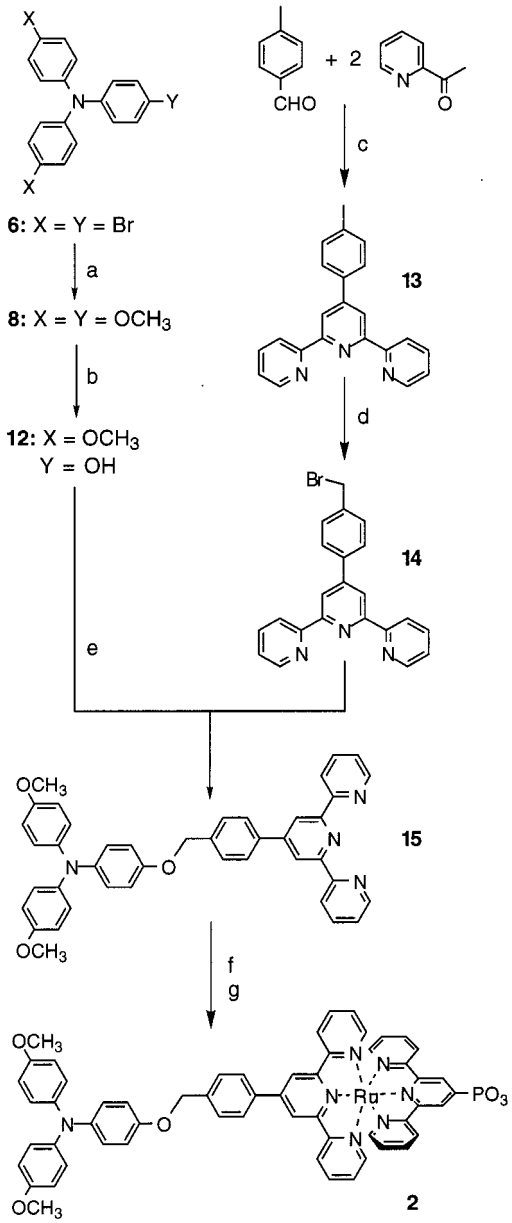


[a] 3 equiv of MeONa, CuI/collidine-MeOH, 14 h reflux (70%); (b) concentrated HBr/AcOH reflux 20 min (33%); (c) $CH_3COONH_4$/$CH_3CONH_2$ reflux 4 h, $Fe^{2+}$ complexation, $H_2O_2$/NaOH (23%); (d) NBS, (Ph-COO)$_2$/benzene, 18 h at reflux (85%); (e) tert-BuOK/THF (48%); (f) $RuCl_3 \cdot 3H_2O$/EtOH (86%); (g) terpy$PO_3Na_2$/NMP-$NEt_3$-EtOH 24 h 110 °C (25%).

dyad **2**, the latter potential could not be measured, since the irreversible second oxidation of the triarylamine moiety ($E_{1/2}$ = 1.39 V for **8**) occurs in the same range. The value should be similar to those measured for complexes **1**, **5**, and **18**. In **18**, the return wave of the second terpy reduction forms a spike, denoting that the bis-reduced complex precipitated on the electrode. For **1** and **2**, only the first one-electron reduction was clearly observed. The redox potentials of the triarylamine part of **2** and **3** are very similar to that measured for the free trianisylamine (**8**) ($E_{1/2}$ = 0.79 V). Replacement of one alkoxy group of **8** by the cationic Ru(II)−terpyridine group raises the oxidation potential of the donor part in dyads **1** and **18**. Symmetrically, the strong coupling with the electron-donating dianisylaminophenyl group lowers the reduction potential of the terpyridine ligand of these complexes by comparison with **2**. From the values of Table 1, the driving forces for the charge-

**Table 1.** Electrochemical Redox Potentials, $E_{1/2}$ in V vs NHE, of Compounds **1**−**18**[a]

| compd | $Ru^{3+/2+}$ | $(terpy)_2^{0/-}$ | $(terpy)_2^{-/2-}$ | $D^{+/0}$ |
|---|---|---|---|---|
| **1**[b] | 1.50 | −1.09 | | 0.95 |
| **18**[c] | 1.57 | −1.04 | −1.23 | 0.98 (2e-) |
| **2**[d] | (1.5) | −0.94 | | 0.85 |
| **3**[b,e] | | | | 0.80 |
| **4**[f] | 1.11 | −1.12 | | |
| **5**[f] | 1.36 | −1.05 | −1.31 | |

[a] Reference electrode: Ag/AgCl−saturated NaCl (+0.197 V vs NHE); supporting electrolyte: 0.1 M $NBu_4^+$ $CF_3SO_3^-$; all one-electron processes, except where specified. [b] In propylene carbonate. [c] In acetonitrile. [d] In acetonitrile/DMSO, 9:1. [e] Measured in the surface-confined state, as a monolayer on a $TiO_2$ nanocrystalline electrode.[17] [f] in DMSO.

**Table 2.** Ground-State Absorption Maxima: $\lambda_{max}$/nm ($\epsilon/10^3$ $M^{-1}$ $cm^{-1}$

| compd | LC | LC | MLCT | $D^{+}$ [c] |
|---|---|---|---|---|
| **1**[a] | 274 (45.6) | 311 (46.0) | 500 (23.0) | |
| $\mathbf{1}^{+}$ [b] | | | 486 (19) | 750 (13) |
| **18**[a] | 277 (66.0) | 310 (87.1) | 516 (51.0) | |
| **2**[a] | | | 486 (21.6) | |
| $\mathbf{2}^{+}$ [a] | | | 486 (23) | 720 (22) |
| $\mathbf{3}^{+}$ [a] | | | | 720 (24) |
| **4**[d] | 280 (35.0) | 320 (26.1) | 498 (8.5) | |
| **5**[d] | 276 (37.2) | 312 (51.8) | 482 (15.3) | |
| **16**[e] | 272 (34.2) | 310 (39.2) | 480 (12.5) | |

[a] In acetonitrile. [b] In acetonitrile/propylene carbonate, 96:4. [c] Obtained by electrochemical oxidation in a spectrophotometric cell (see Experimental Section). [d] In ethanol/DMSO, 9:1. [e] In water (pH = 9).

transfer $D-S^+|(e^-_{cb})TiO_2 \rightarrow D^+-S|(e^-_{cb})TiO_2$ can be estimated to be 0.55 V for **1**, 0.65 V for **2**, 0.31 V for **3** + **4**, and 0.56 V for **3** + **5**.

**Absorption, Emission and Resonance Raman Spectroscopy.** The UV−vis absorption spectra of the studied compounds are summarized in Table 2. The UV bands are attributed to the ligand-centered (LC) transitions, and the visible bands correspond to the well-known metal-to-ligand charge transfer (MLCT). The oxidized triarylamine moieties are characterized by an intense absorption in the red, due to the $\pi \rightarrow \pi$ transition in the radical cation.

The substantial bathochromic−hyperchromic effect induced by the triarylamine conjugated to the terpyridine ligand is obvious in the series including complex **5**, dyad **1**, and complex **18**. The effect is attributed rather to an energy-raising of the metal-centered HOMO of the complex due to the electron-donating character of the triarylamine, than to a lowering of the LUMO ($\pi^*$) of the ligand due to the extension of the conjugation. In fact, if the conjugated triarylamine would only lower the $\pi^*$ of the ligand, the absorption of **18** would not be red-shifted compared to **1**. When the electron-donation is suppressed by electrochemical oxidation of the triarylamine moiety ($\mathbf{1}^+$), weakening and blue-shifting of the MLCT band is observed. In dyad **2**, the absence of $\pi$-conjugation between the triarylamine and the Ru−terpyridine chromophore results in a MLCT absorption at shorter wavelength than for **1** and to the insensitivity of this band to the oxidation the triarylamine ($\mathbf{2}^+$).

Complexes **1** and **2** show the typical emission spectra of ruthenium complexes with respective emission maxima at 686 ± 5 nm and 652 ± 5 nm in ethanol (Figure 2). This clearly reflects the energetics displayed by the corresponding MLCT absorption peaks at 505 and 486 nm. Consistent with other complexes[3f] having the terpyridyl ligand, the emission quantum yield is low at $8 \times 10^{-6}$.

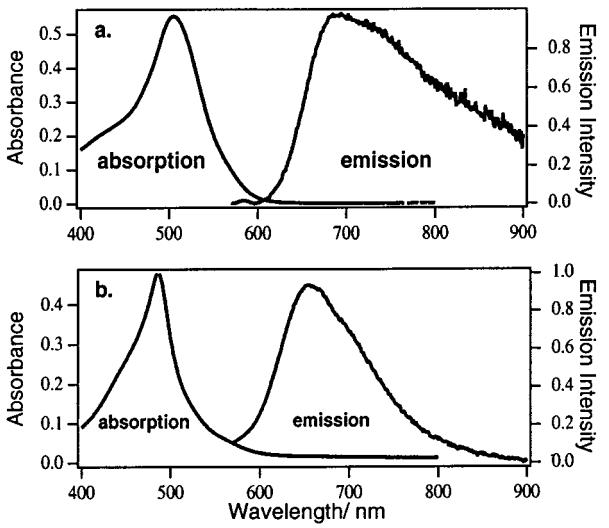


**Figure 2.** Absorption and emission spectra of **1** (a) and **2** (b) 20 $\mu$M in ethanol.

Resonance Raman (RR) spectroscopy was used to elucidate the localization of the electron density upon excitation. Charge transfer from the metal center to a ligand (MLCT) gives rise to resonance enhancements of the symmetric stretching $A_1$ modes of that ligand.[23] For a broad visible absorption spectrum as seen for the heterolyptic complexes **1** and **2** several overlapping MLCT transitions are possible, dictated by the energy of the $\pi^*$ level of the implicated ligand. The relative contribution of each transition can be ascertained by examining the resonant enhancement of the vibrational modes for the different ligands as a function of the probing Raman wavelength. Other groups have demonstrated the utility of this method to map out the MLCT chromophores.[24]

By selecting a wavelength at 530.9 nm, just to the red of the maximum at 504 nm in aqueous **1** (see Figure 2), RR shows a spectrum whose fingerprint in terms of peak position is analogous to that of the ligand **L** (Figure 3). At shorter wavelengths, higher energy electronic states are probed, and the RR spectrum becomes more complex. The set of peaks ascribed to **L** diminish in intensity, while a new set of peaks appear. At 415.4 nm, the RR spectrum resembles the terpy-$PO_3$ ligand fingerprint. It is thus clear that, on the RR time scale ($<10^{-13}$ s), the lowest energy MLCT corresponds to the Ru → **L** transition. When **1** is adsorbed onto the nanocrystalline $TiO_2$ film (**1**|$TiO_2$), the RR clearly shows the same MLCT, even further to the red (568.2 nm) due to less experimental interference from the natural emission of the dye. The terpy$PO_3$ ligand vibrational peaks are also weakly observed at low energies underlying the ligand **L** modes but become dominant at higher energies.

For complex **2**, the RR vibrational spectrum strikingly resembles the spectrum of **16** obtained at 530.9 nm excitation. In that case, the lowest energy MLCT corresponds to the Ru → terpy$PO_3$ transition.

**Charge-Transfer Dynamics.** The transient difference signals of compounds **1**, **2**, **5**, and **3**+**5** adsorbed on nanocrystalline $TiO_2$ films on glass were recorded in different media.

In air, the transient difference spectra obtained upon excitation of heterodyad **5**|$TiO_2$ and heterotriad **1**|$TiO_2$, respectively, were identical. In both cases, excitation at $\lambda = 430$ nm resulted in a

(23) Strommen, D. P.; Mallick, P. K.; Danzer, G. D.; Lumpkin, R. S.; Kincaid, J. R. *J. Phys. Chem.* **1990**, *94*, 1357−1366.

(24) Yabe, T.; Orman, L. K.; Anderson, D. R.; Yu, S.-C.; Xu, X.; Hopkins, J. B. *J. Phys. Chem.* **1990**, *94*, 7128−7132.

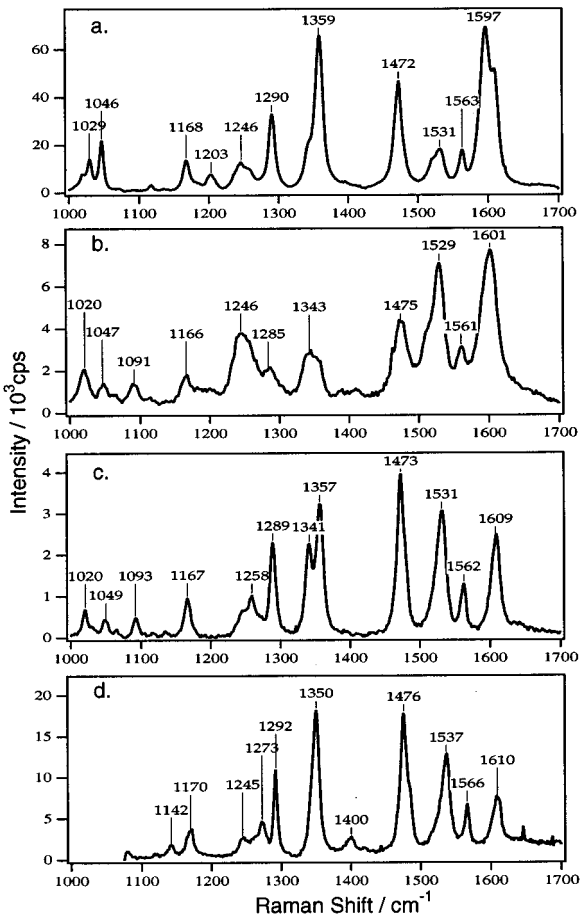


**Figure 3.** Resonance Raman spectra of **1**, using (a) 530.9 nm or (b) 415.4 nm laser excitation, of **2** (c) using 482.5 nm excitation, and of **16** (d) using 530.9 nm excitation.

bleaching of the ground-state absorption of the dye, monitored at 500 nm, concomitantly with the laser pulse. Recovery occurred in the microseconds time scale ($\tau_{1/2} = 3\ \mu$s). The excited-state lifetime of the Ru−terpyridine chromophore being less than 10 ns, the slow recovery of the ground-state absorption is thus interpreted as resulting of a charge injection from the dye MLCT excited state (S*) into the conduction band of the semiconductor (eq 3), followed by the recapture of injected electrons by oxidized dye ($S^+$) at the surface (eq 4).

$$S^*|TiO_2 \rightarrow S^+|(e^-)\ TiO_2 \quad (3)$$

$$S^+|(e^-)\ TiO_2 \rightarrow S|TiO_2 \quad (4)$$

The back electron transfer (eq 4) was found for similar redox sensitizer systems to occur in the microsecond time domain.[11b,25] This slow recombination could be rationalized by considering the large driving force ($\Delta G = -1.5$ eV) for the process, which combined with very small reorganization energies ($\lambda <$ 0.1 eV) characterizing the Ru(II)/Ru(III) exchange in polypyridine complexes,[30] places it deep in the Marcus inverted region. Oxidation of the triarylamine moiety D by $S^+$ in dyad **1**, which is thermodynamically very favorable in propylene carbonate (Table 1), does not take place in air. The medium reorganization is not expected to play an important role in defining the potential of the $S^+/S$ couple in the complex. The absence of solvent then apparently affects the oxidation potential of the amine by increasing its value by more than 0.5 V.

In propylene carbonate (dielectric constant $\epsilon = 64$), the transient signal of heterodyad **5**$|TiO_2$ was the same as that in air. For heterotriad **1**$|TiO_2$, on the contrary, the ground-state absorption of the dye recovered much faster: more than half of the ground-state absorption was regenerated in less than 20 ns (Figure 4a). Simultaneously, a pronounced absorption signal appeared within the laser pulse with a maximum at 750 nm, corresponding to the spectral feature of $D^+$. Quantitative comparison of the initial ground-state bleaching ($\epsilon$(S, 500 nm) $= 2.3 \times 10^4\ M^{-1}\ cm^{-1}$) with the $D^+$ build-up signal ($\epsilon(D^+$, 620 nm) $= 3.5 \times 10^3\ M^{-1}\ cm^{-1}$) shows that 60% of the excited heterotriads underwent intramolecular electron-transfer according to parts a and b of eq 5.

$$D-S^*|TiO_2 \rightarrow D-S^+|(e^-)\ TiO_2 \quad (5a)$$

$$D-S^+|(e^-)\ TiO_2 \rightarrow D^+-S|(e^-)\ TiO_2 \quad (5b)$$

$$D-S^+|(e^-)\ TiO_2 \rightarrow D-S|TiO_2 \quad (5c)$$

Given the long lifetime of the $S^+|(e^-)TiO_2$ state in **5**$|TiO_2$ and the fast appearance of the absorption of $D^+$ within the excitation pulse (eq 5b), the quantum yield for the formation of the radical cation is not likely to be controlled by kinetic competition with charge recombination (eq 4). Oxidation of the donor moiety would therefore be expected to take place quantitatively. For that reason, we cannot formulate a convincing hypothesis for the origin of the low yield of charge separation within the frame of this mechanism. Alternatively to process 5a and 5b, charge separation can take place through reductive quenching of S* by D before charge injection into the solid occurs (eq 6).

$$D-S^*|TiO_2 \rightarrow D^+-S^-|TiO_2 \rightarrow D^+-S|(e^-)\ TiO_2 \quad (6)$$

This mechanism cannot be experimentally distinguished from the previous one in this case since they both take place within the laser pulse and lead to the same final products. However, the moderate yield of charge separation could be explicable on the basis of this second mechanism. Resonance Raman spectroscopy showed that the exicted electron is located on terpy of the ligand **L**, close to the donor. Therefore, the intramolecular charge recombination in the $D^+-S^-$ system could possibly be fast enough to compete efficiently with the electron injection into the semiconductor.

For heterotriad **2**$|TiO_2$ in propylene carbonate, the transient bleaching signal of the ground state of S measured at 500 nm displayed 80% recovery of initial absorption within 10 ns, followed by a second kinetic step that led to complete regeneration 100 ns after the laser pulse. Simultaneously, the absorption of $D^+$ appeared and was monitored at 620 nm. Both signals displayed identical kinetic features with the components $k_1 = 10^8\ s^{-1}$ (80%) and $k_2 = 3 \times 10^7\ s^{-1}$ (20%) (Figure 4a). Using extinction coefficients $\epsilon$(S, 500 nm) $= 1.5 \times 10^4\ M^{-1}\ cm^{-1}$ and $\epsilon(D^+$, 620 nm) $= 6.6 \times 10^3\ M^{-1}\ cm^{-1}$, a unit quantum yield for processes 5a and b is derived. This high efficiency is attributed to the fact that, unlike in **1**, the lowest $\pi^*$ orbital of

(25) O'Regan, B.; Moser, J.; Anderson, M.; Grätzel, M. *J. Phys. Chem.* **1990**, *94*, 8720. Moser, J. E.; Grätzel, M. *Chem. Phys.* **1993**, *176*, 493−500.

(26) Tachibana, Y.; Moser, J. E.; Grätzel, M.; Klug, D. R.; Durrant, J. R. *J. Phys. Chem.* **1996**, *100*, 20056−20062.

(27) Rothenberger, G.; Moser, J.; Grätzel, M.; Serpone, N.; Sharma, D. K. *J. Am. Chem. Soc.* **1985**, *107*, 8054−8059.

(28) Bonhôte, P.; Dias, A. P.; Papageorgiou, N.; Kalyanasundaram, K.; Grätzel, M.; Armand, M. *Inorg. Chem.* **1996**, *35*, 1168−1178.

(29) Pleskov, Y. V. *Solar Energy Conversion*; Springer: Berlin, 1990; pp 8−11.

(30) Sutin, N. *Prog. Inorg. Chem.* **1983**, *30*, 441−498.

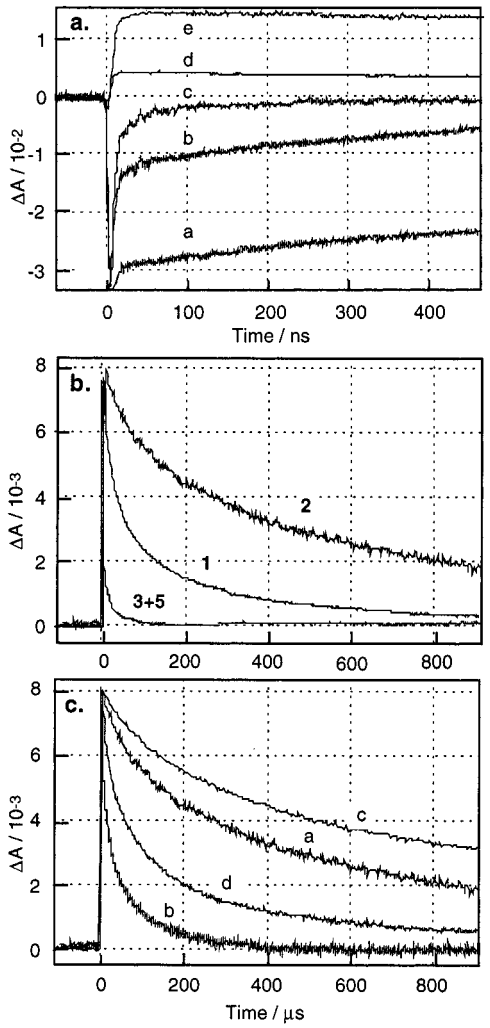


**Figure 4.** Transient absorbance signals recorded upon laser irradiation on nanocrystalline $TiO_2$ films sensitized by adsorption of **1**, **2**, **3** + **5**, and **5** (heterotriads **1**|$TiO_2$, **2**|$TiO_2$, (**3**+**5**)|$TiO_2$, and heterodyad **5**|$TiO_2$). Pulse width = 5 ns, pulse energy = 1.5 mJ. (a) Signals measured in propylene carbonate at $\lambda$ = 500 nm (irradiation at $\lambda$ = 430 nm), corresponding to the temporal evolution of the bleaching of the MLCT ground-state absorption of the chromophore S: [a] **5**|$TiO_2$, [b] **1**|$TiO_2$, and [c] **2**|$TiO_2$; signals measured at $\lambda$ = 750 nm, corresponding to the temporal evolution of the absorption of the radical cation of the donor ($D^+$) moiety of the heterotriads: [d] **1**|$TiO_2$ and (e) **2**|$TiO_2$. (b) Signals of $D^+$ measured in propylene carbonate at $\lambda$ = 620 nm (irradiation at $\lambda$ = 480 nm) with heterotriads **1**|$TiO_2$, **2**|$TiO_2$, and **3**+**5**|$TiO_2$, respectively. The observed decays are due to the recombination of the $D^+$ radical cation species with electrons injected in the conduction band of the semiconductor. (c) Signals of $D^+$ measured at $\lambda$ = 620 nm (irradiation at $\lambda$ = 480 nm) with **2**|$TiO_2$ in two different media, at complete and half monolayer coverage respectively: [a] propylene carbonate, 100% surface coverage; [b] same medium, 50% surface coverage; [c] 1-ethyl-2-methylimidazolium bis(trifluoromethane)sulfonimide, 100% surface coverage; [d] same medium, 50% surface coverage. Absorbance changes were normalized to the same initial amplitude.

the system belongs to the terpy$PO_3$ ligand which anchors onto the $TiO_2$ surface, resulting in an efficient electronic coupling between the excited-state S* and the semiconductor acceptor levels. The observed rate for hole-transfer process (eq 5b) is orders of magnitude smaller than for the electron injection (eq 3) from an efficient sensitizer.[26] This consideration, combined with the absence of spectral detection of the $D^+-S^-|TiO_2$, allows for the exclusion of process 6 as a possible oxidation pathway of the amine besides 5a and b. The lower rate for the latter step in heterotriad **2**|$TiO_2$ compared with that in **1**|$TiO_2$ is attributed to a larger D−S distance. The hole transfer remains, however, much faster than the charge recombination (eq 5c). The biphasic kinetics observed can be due to the multiplicity of the conformations of the molecule that result in different D−S distances or to the existence of intermolecular $D \rightarrow S^+$ electron transfers inside the monolayer.

For heterotriad (**3**+**5**)|$TiO_2$ (**3** and **5** coadsorbed in a 1:1 ratio), the transient spectra recorded upon pulse excitation at 480 nm was very similar as with **2**|$TiO_2$. The fast recovery of the ground-state absorption of the dye within the laser pulse was mirrored by the immediate appearance of the transient absorption of $\mathbf{3}^+$ in the red part of the spectrum. They could not be time-resolved in our experimental setup. This observation is interpreted in terms of a similar electron-transfer sequence as in **2**|$TiO_2$ (eqs 7 and 8).

$$(D + S^*)|TiO_2 \rightarrow (D + S^+)|(e^-)\ TiO_2 \qquad (7)$$

$$(D + S^+)|(e^-)\ TiO_2 \rightarrow (D^+ + S)|(e^-)\ TiO_2 \qquad (8)$$

Comparison of the transient signals ($\epsilon$(**5**, 500 nm) = $10^4$ $M^{-1}$ $cm^{-1}$ and $\epsilon$($\mathbf{3}^+$, 620 nm) = 7 × $10^3$ $M^{-1}$ $cm^{-1}$) indicates that the quantum yield of these processes is practically unity.

The charge recombination processes 9 between the conduction-band electrons and the oxidized donor $D^+$ were followed in propylene carbonate for heterotriads **1**|$TiO_2$, **2**|$TiO_2$, and (**3**+**5**)|$TiO_2$ by the evolution of the transient absorption at 620 nm (Figure 4b).

$$D^+|(e^-)\ TiO_2 \rightarrow D|TiO_2 \qquad (9)$$

The lifetime of the charge separated state ($\mathbf{3}^+$+**5**)|($e^-$)$TiO_2$ is very similar to that obtained with $\mathbf{5}^+$|($e^-$)$TiO_2$ alone. In an inverted regime, the decrease of the driving force for charge recombination by 0.56 eV and the existence of a large solvent reorganization energy associated with the $D/D^+$ couple should indeed compensate in part for the larger distance over which the charge recombination takes place. The recombination kinetics of the three heterotriads are very dissimilar, with half-lifetime ($\tau_{1/2}$) for the $D^+|(e^-)\ TiO_2$ state of 3 $\mu$s in (**3**+**5**)|$TiO_2$, 30 $\mu$s in **1**|$TiO_2$, and 300 $\mu$s in **2**|$TiO_2$. These values have to be compared to the 3 $\mu$s half-lifetime of the reference heterodyad $\mathbf{5}^+$|($e^-$)$TiO_2$. Using known values for the roughness factor of the nanocrystalline film ($\rho$ = 700), its absorbance after dying ($A_{480\ nm}$ = 0.5), and the incident laser pulse energy (1.5 mJ), the average number of electrons initially injected per individual $TiO_2$ particle (10 nm radius) is estimated to be around $\langle x \rangle_0$ = 50. Correlation between injected electrons in the solid and $D^+$ on the surface being unlikely, such a high average initial occupancy of the semiconductor particles by charge-separated pairs should allow the use of a second-order rate law to describe the kinetics of their recombination.[27] The differences in the recombination rates of the different heterotriads can be correlated with the mean distance separating the amine from the surface of the oxide. Perpendicular attachment of the molecules on the surface would imply D−$TiO_2$ distances of 12, 18, and 24 Å for the heterotriads (**3**+**5**)|$TiO_2$, **1**|$TiO_2$, and **2**|$TiO_2$, respectively (Figure 5). Assuming a typical damping factor $\beta$ = 1.2 $Å^{-1}$ for "through-space" electronic coupling between conduction-band electrons and $D^+$, a decrease of the recombination rate by 1 order of magnitude is expected to correspond to an increase of the mean electron-transfer distance by 1.9 Å. The discrepancy between that value and the 6 Å distance differences expected from perpendicular anchoring can be explained by the fact that, very

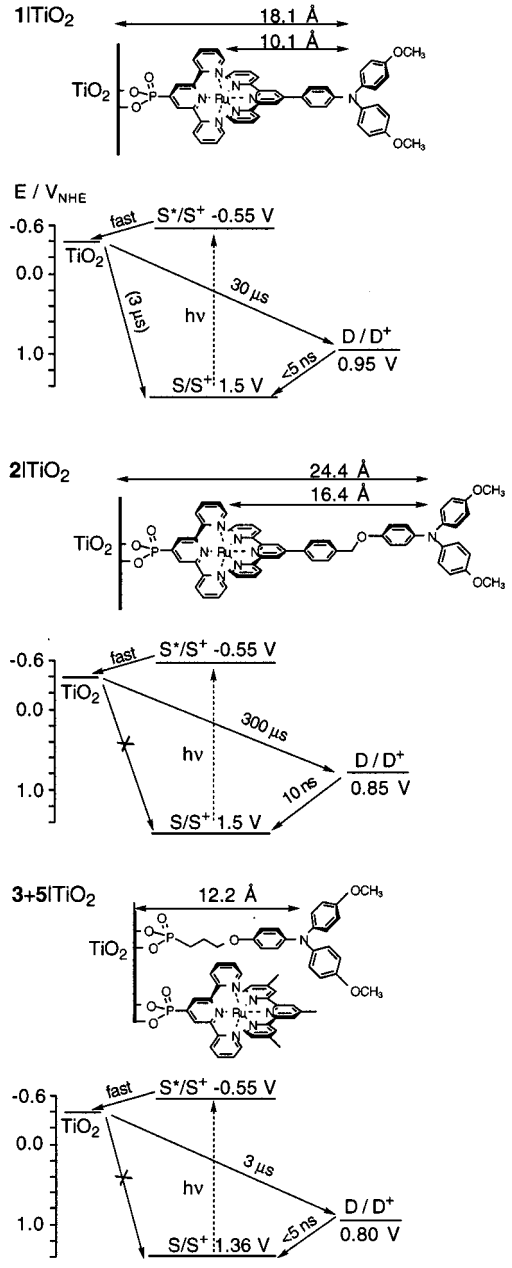


**Figure 5.** Distances, energy levels, and electron-transfer half-lives in the heterotriads **1**|$TiO_2$, **2**|$TiO_2$, and **3**+**5**|$TiO_2$. The distances were calculated by molecular mechanics using CAChe software, assuming a perpendicular arrangement of the molecules on the surface. The energy levels are those obtained and calculated by electrochemistry as well as by absorption and emission spectroscopy. The half-lives for the electron transfers are those obtained by laser flash experiment. The value of 3 $\mu$s for the $S^+|(e^-_{cb})TiO_2 \rightarrow S|TiO_2$ recombination was obtained with the heterodyad **5**|$TiO_2$.

likely, a large portion of adsorbed molecules adopt a tilted conformation on the surface, leading to a broad distribution of distances for the electron transfer 9, and hence to a complex kinetic behavior. In fact, attempts to fit the observed temporal curves demonstrated that they are multiphasic, certainly because the adsorption geometry of the molecules is not fixed. This geometry is likely to be dependent on the surface coverage. In a compact monolayer, perpendicular anchoring should be favored, whereas molecules widely dispersed on the surface should be freer to lean over. It was indeed observed for all three heterotriads that the rate of the recombination reaction 9 depends drastically on the surface concentration. A surface coverage corresponding to 50% of a full monolayer was acheived by brief bathing of the $TiO_2$ nanocrystalline films in the sensitizer solution, until absorbance at 480 nm was 0.25. Upon irradiation by a laser pulse of fixed energy, this partial covering implies a 50% reduction of the number of charge-separated pairs. Considering a second-order kinetic law, the rate of recombination is expected to decrease accordingly. It was observed on the contrary (Figure 4c) that the slowest kinetic components measured for **2**|$TiO_2$ at surface saturation disappeared under partial coverage conditions, while $\tau_{1/2}$ was reduced by more than an order of magnitude. An effect of the same amplitude was observed with heterotriads **1**|$TiO_2$ and (**3**+**5**)|$TiO_2$**.** A more detailed study of this phenomenon, which is attributed to a change in the geometry associated with the electron-transfer process, is currently underway and will be reported elsewhere.

Heterotriad **2**|$TiO_2$ represents obviously the most promising system for long-lived charge separation. In an attempt to further increase the lifetime of $\mathbf{2}^+|(e^-)TiO_2$ state, the photodynamics was studied in the ambient temperature liquid salt 1-ethyl-2-methylimidazolium bis(trifluoromethylsulfonyl)imide[28] which was shown to behave at the molecular scale like a solvent of low dielectric constant ($\epsilon \leq 10$), where the medium reorganization energy should be minimized. Figure 4c shows that the charge recombination process 9 was indeed slowed significantly, with a $\tau_{1/2}$ twice as long as that in propylene carbonate. A very long tail in the kinetic curve, accounting for a few percent of the initial absorbance, was even found to extend up to several hundreds of milliseconds ($\tau_{1/4} = 5$ ms, $\tau_{1/8} = 120$ ms). Interestingly, carefully degassing the molten salt by successive freeze−pump−thaw cycles did not affect this long time kinetic phase, indicating that removal of the conduction-band electrons by molecular oxygen was not competing with the charge recombination.

**Photochromism.** Heterotriads **1**|$TiO_2$, **2**|$TiO_2$, and (**3**+S)|$TiO_2$ display redox-type photochromism. When electrodes made of transparent, nanocrystalline $TiO_2$ film on conducting glass were derivatized by a monolayer of the diads **1**, **2**, **3**+**4**, or **3**+**5**, their absorption spectrum could be changed by the combined action of visible light and applied potential. If the applied potential is maintained higher than the conduction-band level of the semiconductor, but still lower than the redox potential of the triarylamine moiety, then the electron−hole pairs created by the photoinduced charge separation process $D-S|TiO_2 \rightarrow\rightarrow D^+-S|(e^-_{cb})TiO_2$ can no longer recombine. Figure 6 shows the change in the absorption spectra that occurred under illumination with white light (intensity $1 \pm 0.2$ sun (AM 1.5)) of the different heterotriad-derivatized electrodes polarized at + 0.50 V. The spectra of the oxidized states were recorded after 10 min illumination, when a steady-state plateau was reached.

If, after reaching the steady state, the electrical circuit was opened, the spectrum of the $D^+-S|TiO_2$ state remained unchanged for days, provided the contacting electrolyte was free of reducing or nucleophilic impurities, for example, the ambient-temperature liquid salt 1-ethyl-2-methylimidazolium bistrifluoromethane sulfonimide.[28]

Rapid reduction $D^+-S|(e^-_{cb})TiO_2 \rightarrow D-S|TiO_2$ to the initial state was achieved by applying a negative potential ($\leq 0$ V) to the electrode in order to pass electrons above the $TiO_2$ conduction band. Even though the system was not yet tested for long-term stability, it appears to sustain at least 10 light-induced oxidation−reduction cycles without degradation of the heterotriads.

For the heterotriad **1**|$TiO_2$, the observed behavior follows the above-described mechanism implying only interfacial electron

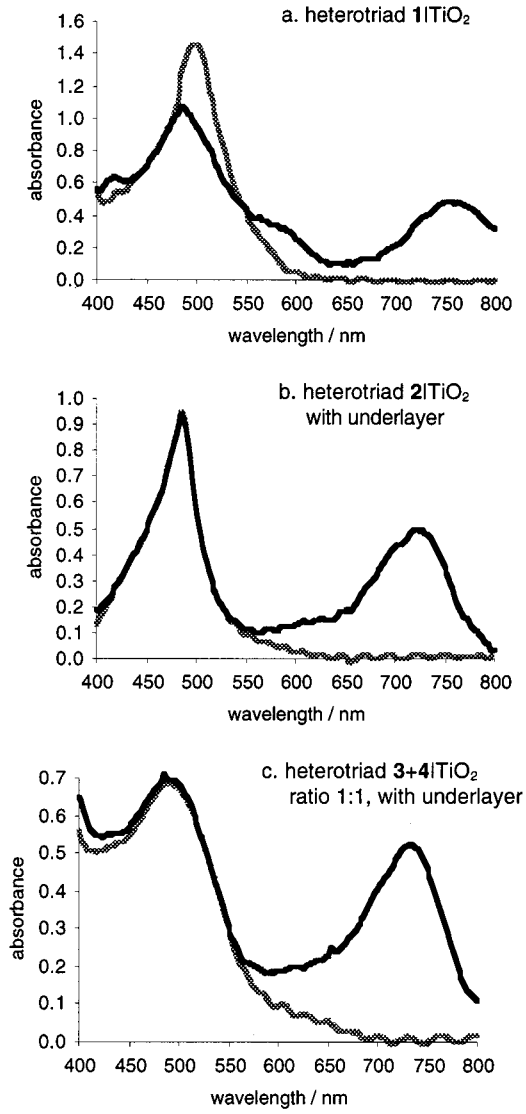


**Figure 6.** Absorption spectra of the heterotriads D−S|$TiO_2$ under positive polarization (0.5 V), in the dark (dotted lines) and after 10 min illumination (full lines). Thickness of the nanocrystalline films: 4.8−5 $\mu$m, roughness factor $400 < \eta < 450$. Interference pattern in the spectra are due to the nanocrystalline layer.

transfer. The absorption spectrum after light-induced oxidation ($D^+$−S|$TiO_2$) resembles that of $\mathbf{1}^+$ in solution (Figure 6a). The ratio *R* between the absorbance of $D^+$ at 752 nm (0.491) and the MLCT absorbance at 486 nm (1.07), hereafter called "photochromic ratio" is 0.46. For $\mathbf{1}^+$ in solution, the absorbance ratio for the same wavelengths is 0.68 (see Table 2). Dividing the former ratio by the latter affords the fraction of the dyad which was oxidized ($D^+$−S|$TiO_2$) in the steady-state, in this case 67%.

For the heterotriad **2**|$TiO_2$, the situation is more complex. If the experiment was carried out as with heterotriad **1**|$TiO_2$, no photochromism was observed. Moreover, if the electrode potential was increased up to 1 V, complete oxidation of **2** to $\mathbf{2}^+$ occurred without illumination, which was manifested by the electrochromism of the electrode. The same electrochromic behavior was observed with nanocrystalline layers of $TiO_2$ derivatized by the phosphonated triarylamine **3**. The phenomenon was attributed to hole injection from the underlying $SnO_2$ to the contacting triarylamine molecules, followed by an efficient charge transfer inside the densly packed self-assembled monolayer of electroactive molecules.[17] Support for this hypothesis

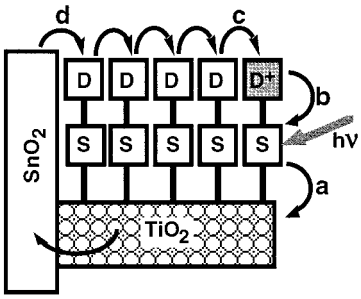


**Figure 7.** Proposed electron fluxes in the illuminated heterotriad **2**|$TiO_2$ on $SnO_2$. Light-induced excitation of the sensitizer S is followed by electron injection (a) into the $TiO_2$ and oxidation (b) of the donor D. Lateral conduction (c) inside the monolayer allows electrons to flow from the $SnO_2$ (d) to the oxidized donors.

**Table 3.** Photochromic Ratio *R* and Oxidized Part of Heterotriad **2**|$TiO_2$ in the Steady State under AM 1.5 Illumination at +0.5 V, as a Function of the Molar Fraction *x* of the Dyad D−S or Donor **3** on the Surface[a]

| heterotriad | underlayer | $x^a$ | $R^b$ | oxidized part[c] |
|---|---|---|---|---|
| **1**\|$TiO_2$ | no | 1.0 | 0.46 | 0.68 |
| **2**\|$TiO_2$ | yes | 1.0 | 0.53 | 0.55 |
| **2**\|$TiO_2$ | yes | 0.5 | 0.57 | 0.59 |
| **2**\|$TiO_2$ | yes | 0.2 | 0.71 | 0.74 |
| **3**+**4**\|$TiO_2$ | no | 0.5[d] | 0.52 | 0.18 |
| **3**+**4**\|$TiO_2$ | yes | 0.5[d] | 0.76 | 0.27 |

[a] *x* on the surface was assumed to be equal to the molar fraction of the relevant molecules to the total concentration of phosphonates in the derivatizing solution. The validity of this assumption was demonstrated previously.[17] [b] Photochromic ratio between the MLCT and the $D^+$ absorbances (see Table 2). [c] By dividing *R* by the corresponding ratio obtained for the corresponding oxidized dyad in solution. [d] Molar fraction of **3**.

was gained from the observation of a percolation threshold when the surface concentration of the electroactive molecules **3** was progressively increased in a monolayer of nonelectroactive coadsorbate. Below a molar fraction $x = 0.5$ of **3**, the monolayer is electrochemically entirely inactive but abruptly becomes active above that limit, with an apparent diffusion coefficient increasing with *x*. Heterotriad **2**|$TiO_2$, with its freely rotating triarylamine, is apparently also able to build hole (or electron)-conducting monolayers. The lateral conductivity efficiently competes with light-induced interfacial oxidation D−S|$TiO_2$ $\rightarrow\rightarrow$ $D^+$−S|($e^-_{cb}$)$TiO_2$, forming a short-circuit according to Figure 7, and thus prevents the appearance of photochromism in the present case. This limitation could be circumvented by deposition of a "compact" $TiO_2$ layer between the $SnO_2$ conducting glass and the nanocrystalline $TiO_2$ film. Such a layer was simply built by dipping the electrode in a $Ti(OBu)_4$ solution followed by hydrolysis in air. Clearly, such a layer is not completely chemically insulating the conducting glass and contains cracks. It sufficiently reduces, however, the contact between the monolayer **2**|$TiO_2$ and the $SnO_2$ to impede the short-circuit reaction, as shown in Figure 6b and Table 3 by the spectacular photochromism of the considered heterotriad in this situation. When dyads **2** were diluted on the surface by the insulating molecules **19**, the photochromic ratio and the steady-state proportion of oxidized **2**|$TiO_2$ *increased* with decreasing concentration (see Table 3) consistently with a reduction of the lateral electron transfer caused by the introduction of the insulating molecules in the monolayer, similarly to what was observed in the monolayers of **3**.

The photochromism observed with the system (**3**+**4**)|$TiO_2$ shows that a chromophore and an electron donor coadsorbed on a surface can form a noncovalently linked dyad, as discussed

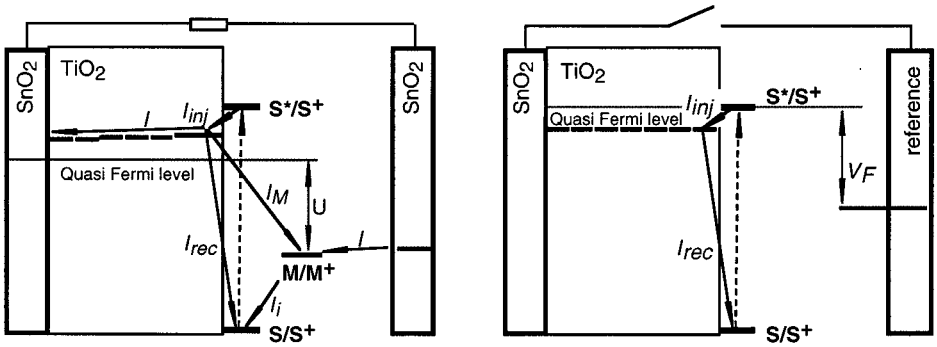


**Figure 8.** Energy levels and electron fluxes in a dye-sensitized solar cell. Left: regenerative cell with redox mediator in solution. Right: setup for measurement of the photopotential versus a reference eletrode, in the absence of redox mediator. S is the dye, M is the redox mediator, $I_{inj}$ is the injection flux, $I_{rec}$ is the recombination flux, $I_M$ is the current flux to $M^+$ and $I$ is the net current delivered by the system.

above in the photodynamics section. Here again, the photochromic steady-state appears to establish as a balance between two opposite fluxes, the light-induced oxidation of **3** and the lateral conductivity allowing electrons to percolate back from the $SnO_2$ to oxidized **3**.

**Photovoltaics.** The link between photodynamics and photovoltaics was established according to the following model, depicted in Figure 8. Under illumination in open circuit, the electrons injected into the $TiO_2$ conduction band at the flux $I_{inj}$ can either recombine with the oxidized sensitizer with the pseudo first-order rate constant $k_{rec}$ or reduce the oxidized redox mediator $M^+$ in solution with the second-order rate constant $k_M$. The steady-state electron density $n$ in the semiconductor is thus given by eq 10. The quasi-Fermi level $F$ of the semiconductor is varying with the electron density according to eq 11, where $E_c$ is the conduction band level and $N_c$ is the effective density of states in the conduction band, a constant value for a given material at a given temperature.[29] The corresponding photopotential $V_F$ of the electrode is obtained by division by the electronic charge $e$ (eq 12). Combining eqs 10 and 12 affords the photopotential as a function of the kinetic parameters (eq 13).

$$n = I_{inj}/(k_{rec} + k_M[M^+]) \quad (10)$$

$$F = E_c - kT\ln(N_c/n) \quad (11)$$

$$V_F = V_c - (kT/e)\ln(N_c/n) \quad (12)$$

$$V_F = V_c - (kT/e)\ln(N_c\ (k_{rec} + k_M[M^+])/I_{inj}) \quad (13)$$

$$\Delta V_F = (kT/e)\ln(k_{recA}I_{injB}/k_{recB}I_{injA}) \quad (14)$$

If two systems **A**|$TiO_2$ and **B**|$TiO_2$, characterized by $k_{recA}$, $I_{injA}$ and $k_{recB}$, $I_{injB}$, respectively, are illuminated in an electrolyte free of redox mediator, then their photopotential difference $\Delta V_F$ can be expressed by eq 14. It must be specified that the laser flash experiment does not afford the pseudo-first-order rate constants $k_{rec}$ but rather rates of the type $k_{rec}' = n'k_{rec}$, since the electron density $n'$ in the semiconductor after the charge injection induced by the laser flash is not exactly known. This density will be taken as identical for all of the considered laser experiments, allowing, consequently, the use of the kinetic values derived from them in eq 14. To account for the multiphasic nature of the decays, synthetic rates corresponding to the first half-lives of the charge-separated states will be considered.

The photopotentials of the three systems **1**|$TiO_2$, **2**|$TiO_2$, and **5**|$TiO_2$ were measured under full sun illumination (AM 1.5) in propylene carbonate with an inert supporting electrolyte (0.1 M tetrabutylammonium triflate). The open-circuit photovoltages versus the $I^-/I_3^-$ redox couple and the short-circuit photocurrents $U_{oc}$ were measured in a regenerative cell, with 1,2-dimethyl-3-propylimidazolium iodide (0.475 M)/triiodide (0.025 M) as electrolyte. The results are presented in Table 4.

**Table 4.** Photopotentials $V_F$ in Absence of Redox Mediator as Well as Open Circuit Photovoltage $I_{sc}$ and Short Circuit Current $I_{sc}$ in a Regenerative Solar Cell with $I^-/I_3^-$ as a Redox Couple[a]

| | **1**\|$TiO_2$ | | **2**\|$TiO_2$ | | **5**\|$TiO_2$ | |
|---|---|---|---|---|---|---|
| $[I^-]$ | $V_F$[b]/$U_{oc}$ | $I_{sc}$[c] | $V_F$[b]/$U_{oc}$ | $I_{sc}$[c] | $V_F$[b]/$U_{oc}$ | $I_{sc}$[c] |
| 0.0 | 729 | 0.0 | 616 | 0.0 | 647 | 0.0 |
| 0.5 | 692 | 2.6 | 612 | 1.2 | 553 | 1.8 |

[a] Average of two electrodes; 10 $\mu$m nanocrystalline $TiO_2$ on "compact" $TiO_2$ on $SnO_2$ conducting glass; estimated uncertainty: ±20 mV. Solvent: propylene carbonate. [b] In mV vs NHE; estimated uncertainty: ±20 mV. [c] In mA/cm$^2$.

Heterotriad **1**|$TiO_2$ gave an 82-mV higher photopotential than **5**|$TiO_2$. This observation can only be in part (58 mV) accounted for by the 10-fold reduced recombination rate. Another contribution of 10 mV is expected from the 50% higher injection flux $I_{inj}$ of the former system in polychromatic light inferred from the values of $I_{sc}$ in the regenerative cell and due to the wider absorption spectrum.

Despite a 100-fold lower recombination rate compared with **5**|$TiO_2$, expected to show itself by a 116-mV gain, the heterotriad **2**|$TiO_2$ gave the lowest photopotential of the series. This observation must be related to a supplementary contribution to $I_{rec}$ represented by the short-circuiting pathway described above, constituted by the lateral charge percolation from triarylamine to triarylamine and finally to the $SnO_2$. It was in fact shown that a monolayer of the model compound **3** on a 5-$\mu$m thick nanocrystalline $TiO_2$ film on conducting glass is able to sustain currents as high as 5 mA/cm$^2$ of electrode at 1.0 V.

In a regenerative solar cell, with the $I^-/I_3^-$ redox couple, the open circuit photovoltage of **1**|$TiO_2$ was now 139 mV higher than that of **5**|$TiO_2$. This increased difference can be attributed to a reduced electron−triiodide reaction flux ($I_M$). In fact, in a regenerative cell in open-circuit, recombination is no longer the only way of escape for the electrons in the conduction band, since they can also reduce the oxidized mediator in solution. The measured values of $I_M$ in the dark, under 550 mV reverse bias were 6.8 mA/cm$^2$ with **5**|$TiO_2$ but only 4 mA/cm$^2$ with **1**|$TiO_2$ and 3.4 mA/cm$^2$ with **2**|$TiO_2$, probably as a result of a restricted access of the triiodide ions to the semiconductor caused by the presence of the bulky triarylamine groups. Heterotriad **2**|$TiO_2$, which photopotential was 31 mV lower than **5**|$TiO_2$, affords in the regenerative cell a 59 mV higher

**Table 5.** Photovoltaic Quantum Yield at 550 nm of Heterotriad **2**|$TiO_2$

| $x^a$ | absorption[b] (%) | IPCE[c] (%) | quantum yield (%) |
|---|---|---|---|
| 1.00 | 77 | 37 | 48 ± 2 |
| 0.80 | 44 | 32 | 73 ± 4 |
| 0.65 | 30 | 24 | 81 ± 6 |
| 0.50 | 24 | 24 | 100 ± 8 |
| 0.20 | 20 | 19 | 96 ± 9 |

[a] Molar fraction on the surface. See remark in Table 3. [b] Light absorption due to **2** at 550 nm, average of 3 points of the electrode. Estimated nonsystematic error: ±1% of absorption. [c] Incident photon to current efficiency at 550 nm. Estimated nonsystematic error: ±1% of IPCE. Electrolyte: 1 M LiI, 0.01 M $LiI_3$ in propylene carbonate.

photopotential, very likely because, in addition to a lower $I_M$, the reduction of $\mathbf{2}^+|TiO_2$ by iodide competes with the lateral electron transfer.

To further elucidate the limiting effect of the lateral electron transfer on the photovoltaic performance of the heterotriad **2**|$TiO_2$, the quantum yield of the whole charge separation process (eq 5a and b) was measured in a mixed monolayer of **2** and **19**. That value which can be regarded as the number of electrons delivered by one molecule in the electrical circuit per 100 absorbed photons, was obtained by dividing the IPCE recorded at a wavelength (550 nm) where no saturation occurs ($A < 1$), by the fraction of absorbed light. It appears clearly (Table 5) that this yield increased with the surface dilution, which can be attributed to the concomitant reduction of the recombination caused by the lateral electron transfer, when the dye molecules are moved away from each other.

## Conclusions

Photoinduced charge separated states reaching half-life times of 300 $\mu$s were achieved by combining intramolecular and interfacial electron transfer. Spectroelectrochemistry, resonance Raman spectroscopy, and laser flash photolysis have allowed detailed understanding of the relevant parameters governing the charge separation and recombination processes in the considered heterotriads, opening the way to an improved efficiency of the light-to-electricity conversion process in the dye-sensitized nanocrystalline solar cell. The efficiency of the photoinduced charge separation was shown by comparison between heterotriads **1**|$TiO_2$ and **2**|$TiO_2$ to depend on the localization of the electron in the excited state of the chromophore, the best yield being obtained with the latter system in which that localization occurs on the ligand bound to the semiconductor surface. Thus, not only the energy levels of the D and S moieties of the heterotriad must be adjusted to allow the charge separation, but also the geometry of the LUMO of S must be considered.

The lifetime of the charge-separated state is controlled by the distance between the electron donor and the surface of the semiconductor. This distance could be further increased in new heterotriads as, even in **2**|$TiO_2$, the hole-transfer process (eq 5b) is still much faster than the recombination (eq 5c). A long and well-defined D−S distance in the molecular dyad is not, however, a sufficient condition to achieve a long-lived charge separation in the heterotriad. The orientation of the molecules in the monolayer plays a crucial role, and care must be taken that a compact monolayer is obtained, ensuring the largest distance of charge separation.

The efficient lateral charge percolation inside a monolayer of closely packed triarylamine studied in detail in the system **3**|$TiO_2$[17] appears to also occur with **2**|$TiO_2$, opening an important short-circuiting pathway in the photoanode incorporating that heterotriad, leading to poor photovoltaic performances. Therefore, in new dyads, donor groups must be chosen which are not prone to build such conducting assemblies. Alternatively, the electronic contact between the molecular monolayer and the underlying conducting substrate must be interrupted by the intercalation of a compact semiconductor layer between the nanocrystalline film and that of the substrate. On the way to improved dye-sensitized solar cells based on heterotriads, the next step that must be studied is the hole transfer from the oxidized donor to the redox mediator in solution. The process should be at least as efficient as that with the sensitizer alone.

The photoelectrochromism of the photoanode made of the investigated heterotriads constitutes a new phenomenon that opens the way to a new type of application for the nanocrystalline $TiO_2$ films. Self-adapting filters and windows exploiting that property can be conceived. Information storage supports based on the same principle could also be feasible, provided the lateral charge migration inside the monolayer could be blocked.

**Acknowledgment.** This work was supported by the Swiss National Science Foundation (FNRS).

JA981742J